Two-Stage GNN-Based Scalable Access Mode Selection and Power Control for Cell-Free and D2D Heterogeneous Networks

Yanpeng Dai, *Member, IEEE*, Dewen Yan, Ling Lyu, *Member, IEEE*, Yunpeng Ge, Nan Cheng, *Senior Member, IEEE*, Min Sheng, *Fellow, IEEE*, Junyu Liu, *Member, IEEE*, and Xuemin Shen, *Fellow, IEEE*

***Abstract*— Cell-free and device-to-device (D2D) heterogeneous networks provide a promising architecture for seamless and high-capacity coverage through dense deployment while reducing fronthaul load. However, spectrum reuse among heterogeneous transmission links would cause severe interference that restricts network capacity and coverage improvement. The dense deployment further challenges efficient interference coordination due to increased computational cost. To this end, this paper proposes a two-stage graph neural network (GNN) structure for access mode selection and power control in cell-free and D2D heterogeneous networks to achieve effective interference coordination with high computational efficiency. First, we derive closed-form expressions for achievable rates of both cell-free and D2D links under limited fronthaul capacity. Then, we represent the network as a heterogeneous graph and design a two-stage GNN based algorithm. The first stage of our proposed algorithm utilizes edge attention mechanism to optimize access mode selection, and its second stage exploits edge message passing to determine power control. To ensure solution feasibility and algorithm convergence, we introduce modified output layers, binary variable regression, and a penalty-based loss function. Simulation results show that our proposed algorithm can improve network capacity and converge to a near-optimal solution across different network scales, compositions, and key parameters, exhibiting well scalability and generalization.**

Received 6 July 2025; revised 29 September 2025; accepted 18 October 2025. Date of publication 28 October 2025; date of current version 31 December 2025. This paper was supported in part by the National Natural Science Foundation of China under Grants 62571081 and 62573082, in part by Doctoral Research Startup Funds of Liaoning Province under Grant 2025-BS-0216, and in part by the Fundamental Research Funds for Central Universities under Grants 3132025259 and 3132025258. The associate editor coordinating the review of this article and approving it for publication was L. P. Qian. *(Corresponding author: Ling Lyu.)*

Yanpeng Dai is with the School of Information Science and Technology, Dalian Maritime University, Dalian 116026, China, and also with the State Key Laboratory of Integrated Services Networks, Xidian University, Xi'an, Shaanxi 710126, China (e-mail: yanpengdai@dlmu.edu.cn).

Dewen Yan, Ling Lyu, and Yunpeng Ge are with the School of Information Science and Technology, Dalian Maritime University, Dalian 116026, China (e-mail: yandewen123@outlook.com; linglyu@dlmu.edu.cn; geyunpeng@dlmu.edu.cn).

Nan Cheng, Min Sheng, and Junyu Liu are with the State Key Laboratory of Integrated Services Networks and the School of Telecommunications Engineering, Xidian University, Xi'an, Shaanxi 710126, China (e-mail: dr.nan.cheng@ieee.org; msheng@mail.xidian.edu.cn; junyuliu@xidian.edu.cn).

Xuemin Shen is with the Department of Electrical and Computer Engineering, University of Waterloo, Waterloo, ON N2L 3G1, Canada (e-mail: sshen@uwaterloo.ca).

Digital Object Identifier 10.1109/TCCN.2025.3626373

***Index Terms*— Cell-free radio access network, device-to-device, power control, mode selection, graph neural network.**

I. Introduction

CELL-FREE massive multiple-input-multiple-output is a promising technique for radio access networks (RANs) to provide seamless and high-capacity coverage [1], [2]. With growing user demands, limited capacity of fronthaul links between access points (APs) and baseband central processing unit (CPU) is becoming the bottleneck of increasing network capacity in cell-free RANs [3], [4]. Device-to-device (D2D) communication is potential to tackle this issue which enables direct transmission between nearby user devices to relieve the load of fronthaul links [5], [6]. However, spectrum reuse among D2D communications and cell-free transmissions would lead to severe local interference to degrade network capacity and coverage [7], [8], [9]. Therefore, effective interference coordination is important to enhance network capacity and spectrum utilization in cell-free and D2D heterogeneous networks.

Dense deployment of APs and D2D transmitters within coverage area is vital for high network capacity in cell-free and D2D heterogeneous networks [10], [11]. However, it poses a challenge for efficient interference coordination. In this heterogeneous network, each user needs to select one access mode between cell-free transmission and D2D communication to avoid severe interference, meanwhile power control for all heterogeneous links is essential for interference mitigation [12], [13]. Traditional optimization methods would have too high computational cost to resolve access mode selection and power control in a large-scale heterogeneous network. Recently, neural network based learning to optimize (L2O) approaches rebuild the paradigm of radio resource and interference management thanks to their high computational efficiency and near-optimal solution [14], [15], [16], [17]. Particularly, graph neural networks (GNNs) exhibit well scalability and generalization, and are hence proposed as underlying model in L2O for wireless network optimization [18], [19], [20]. Hence, it is worthwhile to investigate effective GNN based access mode selection and power control for efficient interference coordination in cell-free and D2D heterogeneous networks.

A. Related Work

Many papers have studied interference coordination in cell-free RANs and D2D communications [21], [22], [23], [24], [25], [26], [27], [28]. For cell-free RANs, Demir and Björnson studied the power control for interference coordination in cell-free RANs with error-free fronthaul links to maximize the minimum of users' spectral efficiency by an alternating optimization algorithm [21]. Mai et al. proposed an iterative power control algorithm based on an accelerated projected gradient method to reduce computational complexity in a large-scale cell-free RANs [22]. Dai et al. investigated the genetic algorithm for interference coordination in cell-free RAN to achieve the tradeoff between the optimality and convergence [23]. Fang et al. studied joint pilot and power allocation by nonlinear programming methods to restrain strong interference in cell-free RANs [24]. For D2D communications in cellular networks, Hamdi et al. optimized power control by Dinkelbach's and conjugate gradient methods to mitigate interference between uplink transmissions and D2D communications [25]. Ramezani-Kebrya et al. proposed a robust power control optimization algorithm for a D2D underlying multi-cell networks [26]. For cell-free and D2D heterogeneous networks, Qiao et al. developed a power control scheme to maximize average sum rate of cell-free downlink transmissions and D2D communications [27]. In this work, closed-form expressions for achievable rates of heterogeneous links are derived without the consideration of fronthaul capacity. Masoumi et al. further proposed graph coloring based pilot allocation and power control strategy to alleviate interference and improve network capacity in cell-free RANs coexisting with D2D communications [28]. The above works propose efficient power control schemes based on traditional optimization methods to maximize network capacity of cell-free and D2D heterogeneous networks and demonstrates the importance of interference coordination on improving network capacity. However, the computational complexity of mostly these optimization methods increases dramatically with the growth of network size, which limits their applicability in large-scale cell-free and D2D heterogeneous networks. Furthermore, most existing works do not consider the influence of fronthaul capacity on transmission performance of cell-free and D2D links coexisting scenarios.

In order to promote computational efficiency, neural network based L2O approaches are increasingly applied to resource and interference management in cell-free transmissions and D2D communications [29], [30], [31], [32], [33]. Shen et al. investigated the architecture design and theoretical analysis of GNNs to solve large-scale radio resource management problems particularly for power control and beamforming in large-scale D2D networks [29]. Guo and Yang proposed to exploit heterogeneous GNNs to learn the optimization of power allocation in multi-cell networks [30]. Shen et al. exhibited that GNN-based power control methods can achieve the near-optimal performance in large-scale D2D networks and cell-free RANs [31]. Luu and Hong developed an adaptive power control algorithm by leveraging GNN model and meta-learning approach to enhance the adaptability to dynamic environments [32]. Yan et al. utilized GNNs to interference coordination in cell-free RANs to achieve near-optimal performance and reduce computational complexity [33]. All the above works demonstrate that GNN-based L2O methods can effectively handle resource and interference management in individual cell-free RANs or D2D networks with near-optimal performance and high computational efficiency. Hence, it is promising to investigate the joint learning and optimization for cell-free and D2D heterogeneous networks. In this case, access mode selection between cell-free transmission and D2D communication for each user is the priority issue to be addressed. Moreover, power control for heterogeneous links is another primary issue to be tackled for efficient interference coordination.

B. Contributions

In this paper, we investigate interference coordination problem in cell-free and D2D heterogeneous networks to increase network capacity. A general architecture of cell-free and D2D heterogeneous network is constructed which includes limited-capacity fronthaul links, uplink training, and cell-free and D2D heterogeneous links. We utilize the spectral efficiency to measure network capacity and formulate a network capacity maximization problem jointly optimizing access mode selection and power control. To tackle this problem, we represent the relationships among all APs, DHs, and users by a heterogeneous graph. Because access mode selections of users are valid prerequisite for power control of all heterogeneous links, a two-stage GNN based algorithm is proposed where its first stage exploits edge attention mechanism to update vertex and edge features to process access mode selection and its second stage utilizes edge message passing to optimize power control. The proposed algorithm is trained in an unsupervised manner. Our main contributions are summarized as follows.

- We derive closed-form expressions for achievable rates of cell-free downlink transmissions and D2D communications, respectively, which jointly consider the impacts of limited fronthaul capacity, interference among heterogeneous transmission links, channel estimation error, and pilot contamination.
- We propose a two-stage GNN based access mode selection and power control algorithm where the first stage utilizes edge attention mechanism to obtain access mode selections, and the second stage exploits edge message passing to acquire power control solutions. Moreover, we introduce a output layer modified by softmax function, binary variable regression to determine access mode selection, and a penalty-based loss function, which guarantee algorithm convergence and solution feasibility. Results show that our proposed algorithm improves network capacity compared to existing neural network-based L2O methods and closely approach advanced optimization algorithm.
- We prove that the designed edge attention and message passing mechanisms enable our two-stage GNN model to achieve permutation invariance and equivariance properties. These properties ensure the scalability and generalization across different network scales, com-

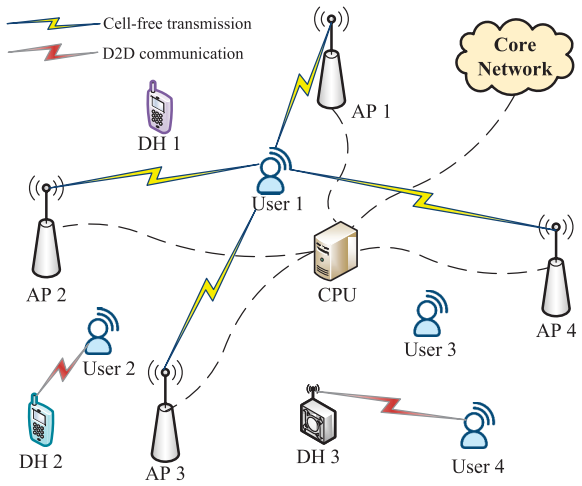

Fig. 1. Cell-free and D2D heterogeneous networks.

positions, and key parameters in cell-free and D2D heterogeneous networks. Simulation results show that our proposed algorithm can converge to a near-optimal solution across various network sizes and scenarios while remaining computationally efficient.

The reminder of this paper is organized as follows. Section II presents the system model and the problem formulation. We propose a two-stage GNN based access mode selection and power control algorithm in Section III. Section IV presents simulation results. Section V concludes this paper.

II. System Model

In this section, we first introduce network model and transmission model. Then, we present the problem formulation of maximizing the capacity of cell-free and D2D heterogeneous networks.

A. Network Model

We consider a cell-free and D2D heterogeneous network which consists of multiple single-antenna users, denoted by $\mathcal{K} = \{1, \ldots, K\}$, and multiple N-antenna APs, denoted by $\mathcal{M} = \{1, \ldots, M\}$, as illustrated in Fig. 1. All the APs are connected to the same baseband CPU via limited-capacity fronthaul links and provide cooperative downlink transmission for all the users in coverage area. Furthermore, there are several D2D helpers (DHs), denoted by $\mathcal{I} = \{1, \ldots, I\}$, which are local transmitters or edge devices in local to establish D2D links with users to provide proximity transmission and alleviate the pressure of fronthaul links. Suppose that each DH is equipped with single antenna and can exchange data and signaling with CPU via dedicated channels.

The channel gain between AP m and user k is represented as $\boldsymbol{g}_{m,k} = \sqrt{u_{m,k}}\boldsymbol{h}_{m,k}$, where $u_{m,k}$ represents the large-scale fading. $\boldsymbol{h}_{m,k} \in \mathbb{C}^{N\times 1}$ is the small-scale fading where independent and identical distributed (i.i.d.) elements follow the distribution $\mathcal{CN}(0,1)$ [34]. Similarly, the channel gain between DH i and user k is represented as $G_{i,k} = \sqrt{v_{i,k}}H_{i,k}$, where $v_{i,k}$ represents the large-scale fading. $H_{i,k} \sim \mathcal{CN}(0,1)$ is the small-scale fading.

Uplink training and time-division duplex mode are conducted in our considered network. Exploiting channel reciprocity, downlink channel condition can be estimated by uplink pilot sequences. During channel estimation, all the users transmit their pilot sequences of length τ_{p} which is less than that of coherence interval [27]. Let $\sqrt{\tau_{\mathrm{p}}}\boldsymbol{\phi}_k \in \mathbb{C}^{\tau_{\mathrm{p}}\times 1}$ denote the pilot sequence transmitted to APs by user k, where $\|\boldsymbol{\phi}_k\| = 1$. The received $N \times \tau_{\mathrm{p}}$ pilot matrix at AP m is expressed as

$$\boldsymbol{y}_m^{\mathrm{c}} = \sqrt{\tau_{\mathrm{p}}\rho_{\mathrm{p}}}\sum_{k=1}^{K}\boldsymbol{g}_{m,k}\boldsymbol{\phi}_k^{\mathrm{H}} + \boldsymbol{n}_m^{\mathrm{c}}, \tag{1}$$

where ρ_{p} is the normalized signal-to-noise ratio (SNR) of each pilot symbol at users [22]. $\boldsymbol{n}_m^{\mathrm{c}} \in \mathbb{C}^{N\times\tau_{\mathrm{p}}}$ is the additive noise with i.i.d. elements following $\mathcal{CN}(0,1)$. The projection of $\boldsymbol{y}_m^{\mathrm{c}}$ onto $\boldsymbol{\phi}_k$ is expressed as $\hat{\boldsymbol{y}}_{m,k}^{\mathrm{c}} = \boldsymbol{y}_m^{\mathrm{c}}\boldsymbol{\phi}_k$. Thus, the minimum mean square error (MMSE) estimation of $\boldsymbol{g}_{m,k}$ is given by

$$\hat{\boldsymbol{g}}_{m,k} = \frac{\mathbb{E}\left\{\left(\hat{\boldsymbol{y}}_{m,k}^{\mathrm{c}}\right)^{*}\boldsymbol{g}_{m,k}\right\}}{\mathbb{E}\left\{\left|\hat{\boldsymbol{y}}_{m,k}^{\mathrm{c}}\right|^2\right\}}\hat{\boldsymbol{y}}_{m,k}^{\mathrm{c}} = c_{m,k}^{\mathrm{a}}\hat{\boldsymbol{y}}_{m,k}^{\mathrm{c}}, \tag{2}$$

$$c_{m,k}^{\mathrm{a}} = \frac{\sqrt{\tau_{\mathrm{p}}\rho_{\mathrm{p}}}u_{m,k}}{\tau_{\mathrm{p}}\rho_{\mathrm{p}}\sum_{k'=1}^{K}u_{m,k'}\left|\boldsymbol{\phi}_{k'}^{\mathrm{H}}\boldsymbol{\phi}_k\right|^2 + 1}. \tag{3}$$

The received $1 \times \tau_{\mathrm{p}}$ pilot vector of DH i is expressed as

$$\boldsymbol{y}_i^{\mathrm{d}} = \sqrt{\tau_{\mathrm{p}}\rho_{\mathrm{p}}}\sum_{k=1}^{K}G_{i,k}\boldsymbol{\phi}_k^{\mathrm{H}} + \boldsymbol{n}_i^{\mathrm{d}}, \tag{4}$$

where $\boldsymbol{n}_i^{\mathrm{d}} \in \mathbb{C}^{1\times\tau_{\mathrm{p}}}$ is the additive noise at DH i. The projection of $\boldsymbol{y}_i^{\mathrm{d}}$ onto $\boldsymbol{\phi}_k$ is expressed as $\hat{y}_{i,k}^{\mathrm{d}} = \boldsymbol{y}_i^{\mathrm{d}}\boldsymbol{\phi}_k$. The MMSE estimation of $G_{i,k}$ is given by

$$\hat{G}_{i,k} = \frac{\mathbb{E}\left\{\left(\hat{y}_{i,k}^{\mathrm{d}}\right)^{*}G_{i,k}\right\}}{\mathbb{E}\left\{\left|\hat{y}_{i,k}^{\mathrm{d}}\right|^2\right\}}\hat{y}_{i,k}^{\mathrm{d}} = c_{i,k}^{\mathrm{d}}\hat{y}_{i,k}^{\mathrm{d}} \tag{5}$$

$$c_{i,k}^{\mathrm{d}} = \frac{\sqrt{\tau_{\mathrm{p}}\rho_{\mathrm{p}}}v_{i,k}}{\tau_{\mathrm{p}}\rho_{\mathrm{p}}\sum_{k'=1}^{K}v_{i,k'}\left|\boldsymbol{\phi}_{k'}^{\mathrm{H}}\boldsymbol{\phi}_k\right|^2 + 1}. \tag{6}$$

B. Transmission Model

We consider the limited-capacity fronthaul links between APs and CPU. In this case, the signal compression is usually urged before signal transmission via fronthaul links, which however leads to the compression quantization noise to degrade the achievable downlink transmission rate. We define the compressed signal as $\hat{s}_{m,k} = s_k + q_{m,k}$ where s_k is the symbol sent to user k and $\mathbb{E}\left\{|s_k|^2\right\} = 1$. $q_{m,k} \sim \mathcal{CN}(0, Q_{m,k})$ is the compression quantization noise and independent of s_k [35]. If the capacity C_m of fronthaul link between AP m and CPU is equally assigned to associated users [36], the compression quantization noise power is expressed as

$$Q_{m,k} = \frac{1}{2^{\frac{C_m}{\sum_{k=1}^{K}\left(1-\sum_{i=1}^{I}\alpha_{i,k}\right)}} - 1}, \tag{7}$$

where $\alpha_{i,k}$ represents the binary variable for access mode selection. $\alpha_{i,k} = 1$ if user k establishes D2D link with DH i. Otherwise, $\alpha_{i,k} = 0$. Each user only selects at most one access mode between cell-free downlink transmission and D2D communication. If one user selects D2D communication, it is just associated to at most one DH.

For cell-free downlink transmission, suppose that channel estimation is treated as true channel and conjugate beamforming is adopted. The signal sent by AP m is expressed as

$$\boldsymbol{x}_m^{\mathrm{c}} = \sqrt{\rho^{\mathrm{c}}} \sum_{k=1}^{K} (1 - \sum_{i=1}^{I} \alpha_{i,k}) \sqrt{\eta_{m,k}^{\mathrm{c}}} \hat{\boldsymbol{g}}_{m,k}^{*} \hat{s}_{m,k}, \tag{8}$$

where ρ^{c} is the normalized downlink SNR at APs. $\eta_{m,k}^{\mathrm{c}}$ represents the positive variable of power control between AP m and user k. Due to the power constraint at each AP, i.e., $\mathbb{E}\left\{\|\boldsymbol{x}_m^{\mathrm{c}}\|^2\right\} \leq \rho^{\mathrm{c}}$ for each AP, $\eta_{m,k}^{\mathrm{c}}$ must satisfy

$$\sum_{k=1}^{K} (1 - \sum_{i=1}^{I} \alpha_{i,k}) \eta_{m,k}^{\mathrm{c}} \gamma_{m,k}^{\mathrm{c}} \leq 1, \tag{9}$$

where $\gamma_{m,k}^{\mathrm{c}} = \mathbb{E}\{\|\hat{\boldsymbol{g}}_{m,k}\|^2\} = N\sqrt{\tau_{\mathrm{p}}\rho_{\mathrm{p}}} u_{m,k} c_{m,k}^{\mathrm{a}}$. For D2D communication, the signal sent by DH i to user k is expressed as $x_{i,k}^{\mathrm{d}} = \sqrt{\rho^{\mathrm{d}} \eta_{i,k}^{\mathrm{d}}} \alpha_{i,k} s_k$, where ρ^{d} is the normalized SNR at DH i and $\eta_{i,k}^{\mathrm{d}}$ is the positive variable of power control between DH i and user k. During data transmission, all APs and DHs simultaneously transmit signals to their associated users. The signal received by user k is expressed as

$$y_k = \sum_{m=1}^{M} \boldsymbol{g}_{m,k}^{\mathrm{T}} \boldsymbol{x}_m^{\mathrm{c}} + \sum_{i=1}^{I} \sum_{k'=1}^{K} G_{i,k} x_{i,k'}^{\mathrm{d}} + n_k^{\mathrm{u}}, \tag{10}$$

where n_k^{u} is the additive noise at user k. Now, we can derive the closed-from expressions of the achievable rate for downlink transmission and D2D communication.

If user k is selected to conduct cell-free downlink transmission, the closed-form expression for its achievable rate is given by Proposition 1.

Proposition 1: In the cell-free and D2D heterogeneous network with conjugate beamforming and signal compression in limited-capacity fronthaul links, the achievable rate of cell-free downlink transmission from all the APs to user k, for any given I, K, M, and N, is expressed as (11)–(14), shown at the bottom of the next page.

Proof: Please refer to Appendix A. □

If user k is selected to conduct the D2D communication, the closed-form expression for its achievable rate is given by Proposition 2.

Proposition 2: In the considered heterogeneous network, the achievable rate of D2D communication from DH i to user k, for any given I, K, M, and N, is expressed as

$$R_k^{\mathrm{d}} = \log_2\big(1 + \frac{\rho^{\mathrm{d}} \sum_{i=1}^{I} \alpha_{i,k} \eta_{i,k}^{\mathrm{d}} v_{i,k}}{I_k^{\mathrm{d}} + Q_k^{\mathrm{d}} + 1}\big), \tag{15}$$

$$I_k^{\mathrm{d}} = \rho^{\mathrm{d}} \sum_{k' \in \mathcal{K} \setminus k} \rho^{\mathrm{d}} \sum_{k'=1}^{K} \sum_{i=1}^{I} \alpha_{i,k'} \eta_{i,k'}^{\mathrm{d}} v_{i,k}, \tag{16}$$

$$Q_k^{\mathrm{d}} = \rho^{\mathrm{c}} \sum_{k'=1}^{K} \big(1 - \sum_{i=1}^{I} \alpha_{i,k'}\big) \big[\sum_{m=1}^{M} \eta_{m,k'}^{\mathrm{c}} u_{m,k} \gamma_{m,k'}^{\mathrm{c}} + \big|\phi_{k'}^{\mathrm{H}} \phi_k\big|^2 \big(\sum_{m=1}^{M} \sqrt{\eta_{m,k'}^{\mathrm{c}}} \gamma_{m,k'}^{\mathrm{c}} \frac{u_{m,k}}{u_{m,k'}}\big)^2\big] \big(1 + Q_{m,k'}\big). \tag{17}$$

Proof: Please refer to Appendix B. □

C. Problem Formulation

In this paper, we aim to maximize the network capacity by jointly optimizing access mode selection and power control. Let $\mathbf{A} = \{\alpha_{i,k} \in \{0,1\}, \forall i \in \mathcal{I}, \forall k \in \mathcal{K}\}$ denote access mode selection variables. Let $\mathbf{H} = \{\eta_{m,k}^{\mathrm{c}} \in \mathbb{R}^+, \forall m \in \mathcal{M}, \forall k \in \mathcal{K}\}$ and $\mathbf{\Xi} = \{\eta_{i,k}^{\mathrm{d}} \in \mathbb{R}^+, \forall i \in \mathcal{I}, \forall k \in \mathcal{K}\}$ denote power control variables for APs and DHs, respectively. The network capacity maximization (NCM) problem is formulated as

$$\begin{aligned} (\mathrm{NCM}): \max_{\{\mathbf{A},\mathbf{H},\mathbf{\Xi}\}} \quad & \sum_{k=1}^{K} \big(R_k^{\mathrm{c}} + R_k^{\mathrm{d}}\big) \\ \text{s.t.} \quad & \mathrm{C1}: (9), \ \forall k \in \mathcal{K} \\ & \mathrm{C2}: \eta_{i,k}^{\mathrm{d}} \leq 1, \quad \forall i \in \mathcal{I}, \quad \forall k \in \mathcal{K} \\ & \mathrm{C3}: \sum_{k=1}^{K} \alpha_{i,k} \leq 1, \quad \forall i \in \mathcal{I} \\ & \mathrm{C4}: \sum_{i=1}^{I} \alpha_{i,k} \leq 1. \quad \forall k \in \mathcal{K} \end{aligned}$$

Constraints C1 and C2 are the maximum transmit power constraints for APs and DHs, respectively. Constraints C3 and C4 ensure that each user only can select at most one access mode and each DH can be associated with at most one user. Problem (NCM) is a mixed-integer non-convex problem due to binary variable $\mathbf{A}$ and non-convex objective function [37]. In this paper, we adopt GNN-based L2O approach to solve Problem (NCM).

III. Problem Solution and Algorithm Design

In this section, we first utilize a heterogeneous graph to represent the relationships of all APs, DHs, and users. Based on this, the edge attention GNN (EAGNN) based access mode selection and power control algorithm is designed to find the solution of Problem (NCM), which integrates edge attention mechanism and edge message passing into a two-stage GNN structure. After that, we present the training manner of our proposed EAGNN model and demonstrate several key insights including permutation invariance and equivariance of EAGNN model.

A. Graph Representation

We utilize a heterogeneous graph $G = (\mathcal{V}, \mathcal{E})$ to represent the relationships among all the APs, DHs, and users in the considered cell-free and D2D heterogeneous network, as Fig. 2 shows. There are three types of vertices in G, i.e., $\mathcal{V} = \mathcal{V}_{\mathrm{AP}} \cup \mathcal{V}_{\mathrm{DH}} \cup \mathcal{V}_{\mathrm{UE}}$. $\mathcal{V}_{\mathrm{AP}} = \{v_m^{\mathrm{AP}}, m \in \mathcal{M}\}$,

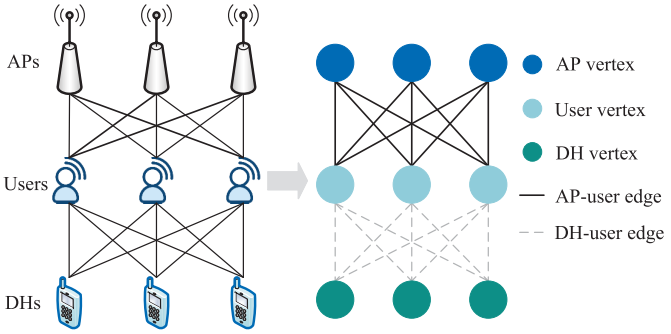

Fig. 2. Graph representation of a cell-free and D2D heterogeneous network.

$\mathcal{V}_{\mathrm{DH}} = \{v_i^{\mathrm{DH}}, i \in \mathcal{I}\}$, and $\mathcal{V}_{\mathrm{UE}} = \{v_k^{\mathrm{UE}}, k \in \mathcal{K}\}$ represent the subsets of AP vertices, DH vertices, and user vertices, respectively. There are two types of edges, i.e., $\mathcal{E} = \mathcal{E}_{\mathrm{AP}} \cup \mathcal{E}_{\mathrm{DH}}$. $\mathcal{E}_{\mathrm{AP}} = \{e_{m,k}^{\mathrm{AP}}, m \in \mathcal{V}_{\mathrm{AP}}, k \in \mathcal{V}_{\mathrm{UE}}\}$ consists of all the edges between AP and user vertices, where each v_m^{AP} in $\mathcal{V}_{\mathrm{AP}}$ has an edge with each v_k^{UE} in $\mathcal{V}_{\mathrm{UE}}$. In other words, all AP vertices in $\mathcal{V}_{\mathrm{AP}}$ form a complete bipartite graph with all user vertices in $\mathcal{V}_{\mathrm{UE}}$. $\mathcal{E}_{\mathrm{DH}} = \{e_{i,k}^{\mathrm{DH}}, i \in \mathcal{V}_{\mathrm{DH}}, k \in \mathcal{V}_{\mathrm{UE}}\}$ consists of all the edges between DH and user vertices. Similarly, all DH vertices in $\mathcal{V}_{\mathrm{DH}}$ form a complete bipartite graph with all user vertices in $\mathcal{V}_{\mathrm{UE}}$. Vertex features are defined as $\mathbf{z}_m^{\mathrm{AP}} \in \mathbb{R}^{l_1}$, $\forall m \in \mathcal{V}_{\mathrm{AP}}$, $\mathbf{z}_i^{\mathrm{DH}} \in \mathbb{R}^{l_1}$, $\forall i \in \mathcal{V}_{\mathrm{DH}}$, and $\mathbf{z}_k^{\mathrm{UE}} \in \mathbb{R}^{l_1}$, $\forall k \in \mathcal{V}_{\mathrm{UE}}$. l_1 is the dimension of vertex features. Edge features are defined as $\boldsymbol{\zeta}_{m,k}^{\mathrm{AP}} \in \mathbb{R}^{l_2}$ and $\boldsymbol{\zeta}_{i,k}^{\mathrm{DH}} \in \mathbb{R}^{l_2}$, $\forall m \in \mathcal{V}_{\mathrm{AP}}$, $\forall i \in \mathcal{V}_{\mathrm{DH}}$, $\forall k \in \mathcal{V}_{\mathrm{UE}}$. G with all features on vertices and edges can be used as the input graph data for a GNN model to extract the desired transmission and interference relationship among different links to promote the solving of Problem (NCM).

B. Model Architecture and Algorithm Design

In this subsection, we propose a two-stage GNN model, i.e., EAGNN model, to solve Problem (NCM). The first stage of EAGNN exploits edge attention mechanism for processing access mode selection, since it can identify which edges in $\mathcal{E}_{\mathrm{AP}}$ or $\mathcal{E}_{\mathrm{DH}}$ can provide more gain for the desired signal transmission. The second stage of EAGNN achieves downlink power control through edge message passing because it can extract global features to restrain interference of entire network. The EAGNN architecture is illustrated in Fig.3. In the initialization phase, $u_{m,k}$ and $v_{i,k}$ are inputted into the embedding layer to generate heterogeneous graph G with initial vertex and edge features. To be specific, edge features $\boldsymbol{\zeta}_{m,k}^{\mathrm{AP}}$ and $\boldsymbol{\zeta}_{i,k}^{\mathrm{DH}}$ are obtained by $\boldsymbol{\zeta}_{m,k}^{\mathrm{AP}} = \boldsymbol{w}_1^{(0)} u_{m,k}$ and $\boldsymbol{\zeta}_{i,k}^{\mathrm{DH}} = \boldsymbol{w}_2^{(0)} v_{i,k}$, respectively, where $\boldsymbol{w}_1^{(0)}$ and $\boldsymbol{w}_2^{(0)}$ are learnable vectors with dimension l_2. Initial vertex features $\mathbf{z}_m^{\mathrm{AP},(0)}$, $\mathbf{z}_i^{\mathrm{DH},(0)}$, and $\mathbf{z}_k^{\mathrm{UE},(0)}$ are obtained by $\mathbf{z}_m^{\mathrm{AP},(0)} = \frac{1}{\sqrt{M}} \boldsymbol{w}_3^{(0)}$, $\mathbf{z}_i^{\mathrm{DH},(0)} = \frac{1}{\sqrt{I}} \boldsymbol{w}_4^{(0)}$, and $\mathbf{z}_k^{\mathrm{UE},(0)} = \frac{1}{\sqrt{K}} \boldsymbol{w}_5^{(0)}$, respectively, where $\boldsymbol{w}_3^{(0)}$, $\boldsymbol{w}_4^{(0)}$, and $\boldsymbol{w}_5^{(0)}$ are learnable vectors with dimension l_1. After the process of the embedding layer, the EAGNN utilizes two individual stages to extract available information for access mode selection and power control.

1) Access Mode Selection: In the first stage of EAGNN, we incorporate edge attention mechanism into a T_1-layer GNN model to update features and use Algorithm 1 to output the result of access mode selection. $\mathcal{N}\left(v_k^{\mathrm{UE}}\right)$ denotes the set of neighbour vertices of vertex v_k^{UE}. The attention value of edge $e_{j,k}$ between v_k^{UE} and $v_j \in \mathcal{N}\left(v_k^{\mathrm{UE}}\right)$ is given by

$$a_{j,k} = \frac{\exp\left(b_{j,k}\right)}{\sum_{j \in \mathcal{N}\left(v_k^{\mathrm{UE}}\right)} \exp\left(b_{j,k}\right)}, \tag{18}$$

$$b_{j,k} = \mathrm{MLP}_1\left(\boldsymbol{\zeta}_{j,k}\right), \tag{19}$$

where $\boldsymbol{\zeta}_{j,k} = \boldsymbol{\zeta}_{j,k}^{\mathrm{AP}}$ if $e_{j,k} \in \mathcal{E}_{\mathrm{AP}}$ and $\boldsymbol{\zeta}_{j,k} = \boldsymbol{\zeta}_{j,k}^{\mathrm{DH}}$ if $e_{j,k} \in \mathcal{E}_{\mathrm{DH}}$. $\mathrm{MLP}_1(\cdot)$ is a learnable multilayer perceptron (MLP) to extract edge features.

At layer t, we aggregate these edge features by mean pooling and combine the aggregated feature with vertex feature of v_k^{UE}, which is expressed as

$$\boldsymbol{\Omega}_k^{\mathrm{UE},(t)} = \frac{1}{\left|\mathcal{N}\left(v_k^{\mathrm{UE}}\right)\right|} \sum_{v_j \in \mathcal{N}\left(v_k^{\mathrm{UE}}\right)} a_{j,k} \boldsymbol{W}_1^{(t)} \boldsymbol{\zeta}_{j,k}, \tag{20}$$

$$\mathbf{z}_k^{\mathrm{UE},(t)} = \boldsymbol{W}_2^{(t)} \boldsymbol{\Omega}_k^{\mathrm{UE},(t)} + \mathbf{z}_k^{\mathrm{UE},(t-1)}, \tag{21}$$

where $\boldsymbol{W}_1^{(t)}$ and $\boldsymbol{W}_2^{(t)}$ are learnable weight matrices at layer t. Meanwhile, $\mathbf{z}_m^{\mathrm{AP},(t)} = \mathbf{z}_m^{\mathrm{AP},(t-1)}$ and $\mathbf{z}_i^{\mathrm{DH},(t)} = \mathbf{z}_i^{\mathrm{DH},(t-1)}$. After the processing of T_1 layers, we can obtain updated vertex feature $\mathbf{z}_k^{\mathrm{UE},(T_1)}$ at layer T_1. In order to enhance the capture of relationships between user k and DHs, edge feature $\boldsymbol{\zeta}_{i,k}^{\mathrm{DH}}$ is updated by $\mathbf{z}_k^{\mathrm{UE},(T_1)}$ at the output layer as

$$\bar{\zeta}_{i,k}^{\mathrm{DH}} = \mathrm{ReLU}\left(\mathrm{MLP}_2\left(\boldsymbol{W}_3^{(T_1)} \mathbf{z}_k^{\mathrm{UE},(T_1)} + \boldsymbol{\zeta}_{i,k}^{\mathrm{DH}}\right)\right), \tag{22}$$

$$R_k^{\mathrm{c}} = \log_2\left(1 + \frac{\rho^{\mathrm{c}} \left|\left(1 - \sum_{i=1}^{I} \alpha_{i,k}\right) \sum_{m=1}^{M} \sqrt{\eta_{m,k}^{\mathrm{c}}} \gamma_{m,k}^{\mathrm{c}}\right|^2}{B_k^{\mathrm{c}} + I_k^{\mathrm{c}} + Q_k^{\mathrm{c}} + 1}\right), \tag{11}$$

$$B_k^{\mathrm{c}} = \rho^{\mathrm{c}}\left(1 - \sum_{i=1}^{I} \alpha_{i,k}\right) \sum_{m=1}^{M} \eta_{m,k}^{\mathrm{c}} \gamma_{m,k}^{\mathrm{c}} u_{m,k} + \rho^{\mathrm{d}} \sum_{k'=1}^{K} \sum_{i=1}^{I} \alpha_{i,k'} \eta_{i,k'}^{\mathrm{d}} v_{i,k}, \tag{12}$$

$$I_k^{\mathrm{c}} = \rho^{\mathrm{c}} \sum_{k' \in \mathcal{K} \setminus k} \left(1 - \sum_{i=1}^{I} \alpha_{i,k'}\right) \left[\left|\phi_{k'}^{\mathrm{H}} \phi_k\right|^2 \left(\sum_{m=1}^{M} \sqrt{\eta_{m,k'}^{\mathrm{c}}} \gamma_{m,k'}^{\mathrm{c}} \frac{u_{m,k}}{u_{m,k'}}\right)^2 + \sum_{m=1}^{M} \eta_{m,k'}^{\mathrm{c}} u_{m,k} \gamma_{m,k'}^{\mathrm{c}}\right], \tag{13}$$

$$Q_k^{\mathrm{c}} = \rho^{\mathrm{c}} \sum_{k'=1}^{K} \left(1 - \sum_{i=1}^{I} \alpha_{i,k'}\right) \left[\left|\phi_{k'}^{\mathrm{H}} \phi_k\right|^2 \left(\sum_{m=1}^{M} \sqrt{\eta_{m,k'}^{\mathrm{c}}} \gamma_{m,k'}^{\mathrm{c}} \frac{u_{m,k}}{u_{m,k'}}\right)^2 + \sum_{m=1}^{M} \eta_{m,k'}^{\mathrm{c}} u_{m,k} \gamma_{m,k'}^{\mathrm{c}}\right] Q_{m,k'}, \tag{14}$$

Algorithm 1 Binary Variable Regression for Access Mode Selection

Initialization
• Initialize matrix $\mathbf{D} \in \mathbb{R}^{I\times K}$, where $\mathbf{D}[i,k] = \bar{\zeta}_{i,k}^{\mathrm{DH}}$.
• Input zero matrix $\bar{\mathbf{A}} \in \mathbb{R}^{I\times K}$ and threshold $\bar{\alpha}$.
for $i = 1, \cdots, I$ **do**
  $k^\star = \arg\max_{k\in\mathcal{K}} \mathbf{D}[i,k]$.
  $\bar{\mathbf{A}}[i,k^\star] = 1$.
end for
for $k = 1, \cdots, K$ **do**
  $\mathcal{I}_k = \{i \in \mathcal{I} \,|\, \bar{\mathbf{A}}[i,k] = 1\}$.
  $i^\star = \arg\max_{i\in\mathcal{I}_k} \mathbf{D}[i,k]$.
  Set $\bar{\mathbf{A}}[i,k] = 0, \forall i \in \mathcal{I}_k \setminus i^\star$.
end for
$\mathcal{A} = \{[i,k] \,|\mathbf{D}[i,k] \le \bar{\alpha}, \forall i \in \mathcal{I}, \forall k \in \mathcal{K}\}$.
Set $\bar{\mathbf{A}}[i,k] = 0, \forall [i,k] \in \mathcal{A}$.
return $\mathbf{A} = \bar{\mathbf{A}}$.

where $\boldsymbol{W}_3^{(T_1)}$ is a learnable weight matrix. $\mathrm{MLP}_2(\cdot)$ is a learnable MLP at layer T_1. The rectified linear unit function (ReLU) is used as the activation function.

We utilize all the $\bar{\zeta}_{i,k}^{\mathrm{DH}}$s to obtain access mode selection results, the detailed procedure of which is summarized in Algorithm 1. To be specific, steps 1-3 are the initialization phase of Algorithm 1 to input matrices $\mathbf{D} = \left[\bar{\zeta}_{i,k}^{\mathrm{DH}}\right]_{I\times K}$, $\bar{\mathbf{A}} = [0]_{I\times K}$ and threshold $\bar{\alpha}$. In steps 4-7, the user $k^\star$ with the maximum $\bar{\zeta}_{i,k}^{\mathrm{DH}}$ for each $i \in \mathcal{I}$ is prior selected and set $\bar{\mathbf{A}}[i,k^\star] = 1$. Steps 8-12 ensure that the elements in matrix $\bar{\mathbf{A}}$ meet constraints C3 and C4. Steps 13 and 14 set $\bar{\mathbf{A}}[i,k] = 0$ if $\bar{\zeta}_{i,k}^{\mathrm{DH}} \le \bar{\alpha}, \forall i \in \mathcal{I}, \forall k \in \mathcal{K}$. Finally, we can obtain access mode selection results, i.e., $\mathbf{A} = \bar{\mathbf{A}}$.

Proposition 3: The aggregation operation in (20) has the permutation invariance property. For any permutation operator π, it can generate a permutation of $\mathcal{N}(v_k^{\mathrm{UE}})$, denoted by $\mathcal{N}\left(v_{\pi(k)}^{\mathrm{UE}}\right)$, which can meet

$$\boldsymbol{\Omega}_{\pi(k)}^{\mathrm{UE},(t)} = \frac{1}{\left|\mathcal{N}\left(v_{\pi(k)}^{\mathrm{UE}}\right)\right|} \sum_{v_{\pi(j)}\in\mathcal{N}\left(v_{\pi(k)}^{\mathrm{UE}}\right)} a_{\pi(j),k} \boldsymbol{W}_1^{(t)} \boldsymbol{\zeta}_{\pi(j),k}, = \boldsymbol{\Omega}_k^{\mathrm{UE},(t)}. \tag{23}$$

Proof: Please refer to Appendix C. □

2) Power Control: In the second stage of EAGNN, edge message passing is used to update vertex and edge features to output power control results. Specifically, the second stage of EAGNN comprises T_2 layers. The initial vertex features of the second stage are the output vertex features of the first stage, i.e., $\{\mathbf{z}_m^{\mathrm{AP},(T_1)}, \mathbf{z}_i^{\mathrm{DH},(T_1)}, \mathbf{z}_k^{\mathrm{UE},(T_1)}, m \in \mathcal{V}_{\mathrm{AP}}, i \in \mathcal{V}_{\mathrm{DH}}, k \in \mathcal{V}_{\mathrm{UE}}\}$. The initial edge features of the second stage are same with that of the first stage, i.e., $\{\boldsymbol{\zeta}_{m,k}^{\mathrm{AP}}, \boldsymbol{\zeta}_{i,k}^{\mathrm{DH}}, m \in \mathcal{V}_{\mathrm{AP}}, i \in \mathcal{V}_{\mathrm{DH}}, k \in \mathcal{V}_{\mathrm{UE}}\}$.

At layer t of the second stage, the feature of vertices in $\mathcal{V}_{\mathrm{AP}}$ and $\mathcal{V}_{\mathrm{DH}}$ are first updated as

$$\boldsymbol{\Omega}_m^{\mathrm{AP},(t)} = \frac{1}{|\mathcal{N}(v_m^{\mathrm{AP}})|} \sum_{v_k^{\mathrm{UE}}\in\mathcal{N}(v_m^{\mathrm{AP}})} \boldsymbol{W}_4^{(t)} \boldsymbol{\zeta}_{m,k}^{\mathrm{AP}}, \tag{24}$$

$$\boldsymbol{\Omega}_i^{\mathrm{DH},(t)} = \frac{1}{|\mathcal{N}(v_i^{\mathrm{DH}})|} \sum_{v_k^{\mathrm{UE}}\in\mathcal{N}(v_i^{\mathrm{DH}})} \boldsymbol{W}_5^{(t)} \boldsymbol{\zeta}_{i,k}^{\mathrm{DH}}, \tag{25}$$

$$\mathbf{z}_m^{\mathrm{AP},(t)} = \boldsymbol{W}_6^{(t)} \boldsymbol{\Omega}_m^{\mathrm{AP},(t)} + \mathbf{z}_m^{\mathrm{AP},(t-1)}, \tag{26}$$

$$\mathbf{z}_i^{\mathrm{DH},(t)} = \boldsymbol{W}_7^{(t)} \boldsymbol{\Omega}_i^{\mathrm{DH},(t)} + \mathbf{z}_i^{\mathrm{DH},(t-1)}, \tag{27}$$

where $\mathcal{N}(v_m^{\mathrm{AP}})$ and $\mathcal{N}(v_i^{\mathrm{DH}})$ are the sets of neighbour vertices of vertices v_m^{AP} and v_i^{DH}, respectively. $\boldsymbol{W}_4^{(t)}$, $\boldsymbol{W}_5^{(t)}$, $\boldsymbol{W}_6^{(t)}$, and $\boldsymbol{W}_7^{(t)}$ are learnable matrices at this layer. (24) and (25) use mean pooling to aggregate connected edge features for v_m^{AP} and v_i^{DH}, respectively. Then, edge features are updated at layer T_2 as

$$\hat{\boldsymbol{\zeta}}_{m,k}^{\mathrm{AP}} = \boldsymbol{W}_8^{(T_2)} \mathbf{z}_m^{\mathrm{AP},(T_2)} + \boldsymbol{\zeta}_{m,k}^{\mathrm{AP}}, \tag{28}$$

$$\hat{\boldsymbol{\zeta}}_{i,k}^{\mathrm{DH}} = \boldsymbol{W}_9^{(T_2)} \mathbf{z}_i^{\mathrm{DH},(t)} + \boldsymbol{\zeta}_{i,k}^{\mathrm{DH}}, \tag{29}$$

where $\boldsymbol{W}_8^{(T_2)}$ and $\boldsymbol{W}_9^{(T_2)}$ are learnable matrices. After that, edge features are inputted into a output layer modified by sigmoid function to obtain the results of power control. The modified output layer is expressed as

$$\eta_{m,k}^{\mathrm{c}} = \frac{1}{\gamma_{m,k}^{\mathrm{c}}} \mathrm{sigmoid}\left(\mathrm{MLP}_3\left(\hat{\boldsymbol{\zeta}}_{m,k}^{\mathrm{AP}}\right)\right), \tag{30}$$

$$\eta_{i,k}^{\mathrm{d}} = \mathrm{sigmoid}\left(\mathrm{MLP}_4\left(\hat{\boldsymbol{\zeta}}_{i,k}^{\mathrm{DH}}\right)\right), \tag{31}$$

where the sigmoid function is used as the activation function. $\mathrm{MLP}_3(\cdot)$ and $\mathrm{MLP}_4(\cdot)$ are learnable MLPs at the output layer. Similar to the first stage of EAGNN, the second stage of EAGNN exhibits permutation invariance due to the mean pooling operator.

According to the design of EAGNN above-mentioned, the optimization of access mode selection and power control by implementing EAGNN is independent of the permutation of vertices in $\mathcal{V}$ of G. Therefore, we can prove that the entire framework of EAGNN exhibits permutation equivariance as shown in the following Proposition 4.

Proposition 4: The proposed EAGNN has the permutation equivariance property. For any permutation π, we have $\mathrm{EAGNN}(\pi \star \mathbf{Z}, \pi \star \mathbf{E}) = \pi \star \mathrm{EAGNN}(\mathbf{Z}, \mathbf{E})$, where $\mathrm{EAGNN}(\cdot)$ is the input-output mapping of EAGNN. $\mathbf{Z}$ is vertex feature matrix including all the features of vertices in $\mathcal{V}$ and $\mathbf{E}$ is edge feature matrix including all the features of edges in $\mathcal{E}$.

Proof: Please refer to Appendix D. □

The computational complexity of our proposed EAGNN algorithm is analyzed as follows. Because the hyperparameters of our proposed two-stage GNN model, such as the dimension of initial features and the width of hidden layer in MLPs, are independent of network scale, we focus on the impacts of I, M, and K on computational complexity. The first stage of EAGNN algorithm is with the complexity of $O\left(K(M+I)^2\right)$ and its second stage is with the complexity of $O\left(K(M+I)\right)$. Therefore, the computational complexity of our proposed EAGNN algorithm is $O\left(K(M+I)^2\right)$.

C. Model Training

The proposed EAGNN model is trained in an unsupervised manner. The penalty method is used to incorporate constraint

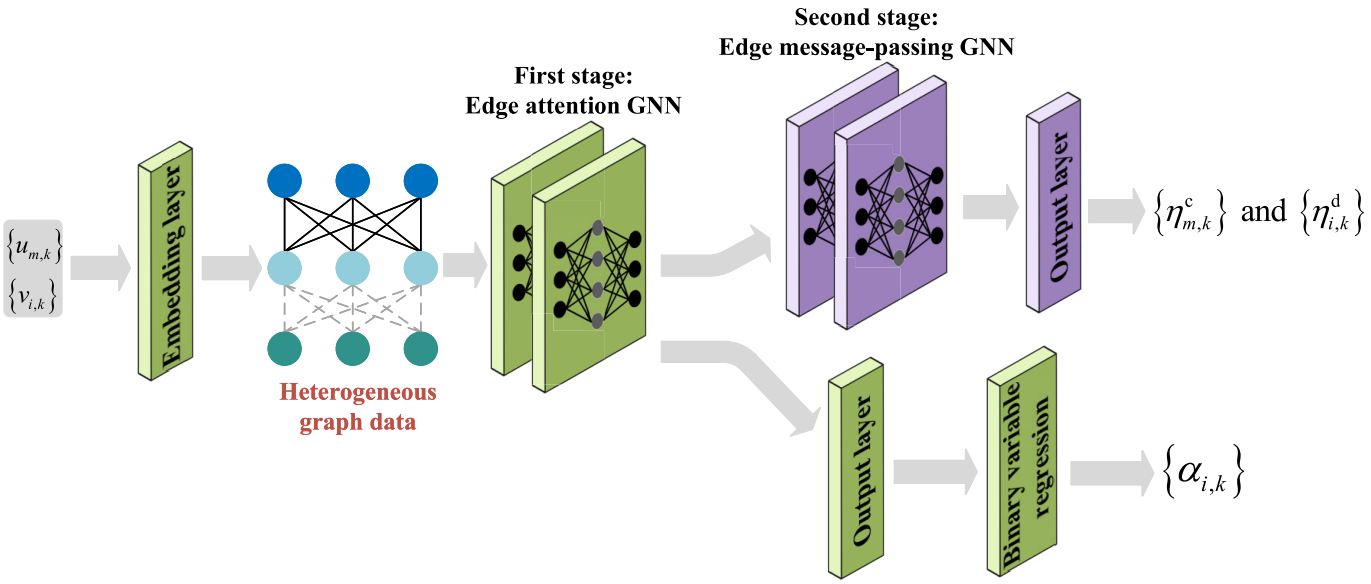

Fig. 3. Proposed EAGNN to jointly optimize access mode selection and power control in considered cell-free and D2D heterogeneous network.

C1, i.e. (9), into the loss function, which ensures the output of EAGNN to be feasible for Problem (NCM). Let Θ denote all learnable parameters of EAGNN including all learnable vectors, matrices and MLPs. The penalty-based loss function is defined as

$$\begin{aligned} L(\Theta) = -\sum_{k=1}^{K}\big(&R_k^{\mathrm{c}}(\mathbf{A}(\Theta),\mathbf{H}(\Theta),\boldsymbol{\Xi}(\Theta)) \\ &+ R_k^{\mathrm{d}}(\mathbf{A}(\Theta),\mathbf{H}(\Theta),\boldsymbol{\Xi}(\Theta))\big) \\ &+ \lambda\Big(\sum_{k=1}^{K}(1-\sum_{i=1}^{I}\alpha_{i,k})\eta_{m,k}^{\mathrm{c}}(\Theta)\gamma_{m,k}^{\mathrm{c}}-1\Big), \end{aligned} \quad (32)$$

where $\mathbf{A}(\Theta)$, $\mathbf{H}(\Theta)$, $\boldsymbol{\Xi}(\Theta)$, and $\eta_{m,k}^{\mathrm{c}}(\Theta)$ are the output results of access mode selection and power control by solving Problem (NCM) when EAGNN is parameterized by Θ. λ is the penalty coefficient and treated as a hyperparameter. During the model training, the EAGNN learns to adjust its parameters Θ to minimize the value of loss function in an unsupervised manner via stochastic gradient descent method [38]. Θ is updated as $\Theta = \Theta - \omega\nabla_{\Theta}L(\Theta)$, where ω is the learning rate.

D. Key Insights

Our proposed EAGNN algorithm is efficient to tackle the access mode selection and power control problem shown as Problem (NCM) in cell-free and D2D heterogeneous networks, due to its design properties and insights discussed as follows.

1) Effectiveness to Capture Heterogeneous Relationships: Our proposed EAGNN can effectively capture the relationships among heterogeneous vertices, i.e., v_m^{AP}s, v_i^{DH}s, and v_k^{UE}s. These heterogeneous relationships are integrated into our constructed graph data and GNN structure. To be specific, we embed large-scale fadings $u_{m,k}$s and $v_{i,k}$s into edge features, which is different from existing works [31], [39]. Thus, edge feature aggregations, i.e., (21), (24), and (25), capture not only the desired signal strength but also the interference intensity. Furthermore, each vertex can gradually require global conditions of transmission and interference links via multi-layer message passing and feature updates, i.e., (20), (26), and (27). This design property is favorable for EAGNN to produce a feasible access mode selection and power control solution to effectively coordinate interference and increase network capacity.

2) Permutation Invariance and Equivariance: Our proposed EAGNN exhibits the properties of permutation invariance and equivariance. Specifically, the permutation invariance property ensures the output of each layer of every stage of EAGNN is unchanged if the vertex ordering is permuted, as shown in Proposition 3 and its proof in Appendix C. When the permutation invariance is met at each layer of every stage of EAGNN, the entire structure of EAGNN shows the permutation equivariance property, i.e., the output of EAGNN is equivalently varied with respect to the permutation of vertices, as shown in Proposition 4 and its proof in Appendix D. These properties enable the EAGNN can be feasible to process a graph data of a given G without any specific labeling for any AP, DH, or user, which significantly reduces computational requirements.

3) Scalability to the Size of Heterogeneous Network: Our proposed EAGNN has well scalable to the size of cell-free and D2D heterogeneous networks. Once the EAGNN model is trained, it can be used to solve the access mode selection and power control problem as shown in Problem (NCM) with different sizes of cell-free and D2D heterogeneous networks. This is because that in EAGNN model structure, message passing mechanism, feature aggregation and combination operations, the dimensions of learnable parameters and other aspects are independent of I, K, and M. This property can greatly facilitate computational efficiency and implementation of EAGNN.

IV. Simulation Results

In this section, we conduct simulations to evaluate the performance of our proposed EAGNN algorithm. The default setting of network scale is $I = 10$ DHs, $K = 10$ users, and $M = 20$ APs with $N = 2$ antennas. All the APs and users

TABLE I
DEFAULT SIMULATION PARAMETERS

Parameter	Value
Network scale I, K, M, N	10, 10, 20, 2
Normalized SNRs ρ_{p}, ρ^{c}, ρ^{d}	200 mW, 200 mW, 100 mW
Length of pilot sequence, τ_{p}	20 samples within 200 samples of coherent interval
Fronthaul capacity, C_m	20 bps/Hz
Model depth, T_1, T_2	2, 2
Initial learning rate, ω	5×10^{-4}

are uniformly distributed in an area of $1 \times 1\mathrm{km}^2$. DHs are randomly distributed around users. The multi-slope path loss model in [12] and [22] is used to characterize $u_{m,k}$ and $v_{i,k}$. The maximum transmit powers, i.e., the normalized SNR at transmitters, are set as $\rho_{\mathrm{p}} = \rho^{\mathrm{c}} = 200$ mW and $\rho^{\mathrm{d}} = 100$ mW. The length of coherent interval is set as 200 samples and the length of pilot sequence τ_{p} is set as 20 samples. The fronthaul capacity of each AP is 20 bps/Hz. GNN architecture and message passing mechanism design are executed by Pytorch and Deep Graph Library [40], [41]. The Adam optimizer with an initial learning rate $\omega = 5 \times 10^{-4}$ is used in model training process. The depth of our proposed EAGNN is set as $T_1 = T_2 = 2$. The default simulation parameters are concluded in Table I.

In order to validate advantages of our proposed EAGNN, we consider three benchmark algorithms for performance comparison as follows.

- **MLP:** The algorithm exploits the MLP [42] to extract and process vertex and edge features rather than GNNs. Then, it uses the same output layer and method with EAGNN to obtain the result of access mode selection and power control.
- **Heterogeneous GNN (HetGNN):** In this algorithm, a HetGNN model proposed in [30] is used to replace EAGNN to extract vertex and edge features with a three-layer structure. Other aspects in this algorithm are same with EAGNN algorithm.
- **Successive convex approximation (SCA):** In this algorithm, the power control is optimized by an advanced optimization method, i.e., SCA [43], to overcome the non-convexity of Problem (NCM), after access mode selection is given by the first stage of EAGNN.

A. Convergence Performance

Fig. 4 shows the convergence performance of our proposed EAGNN with different values of K. We observe from Fig. 4(a) that our proposed EAGNN achieves the convergence within a limited number of epochs on training and validation datasets under different values of K. The required number of training epochs increases with the growth of K. We can see from Fig. 4(b) that the penalty of EAGNN gradually approaches 0 under different values of K when the convergence is achieved on validation dataset. In this case, the value of loss function is all contributed by network capacity, which demonstrates the solution feasibility of our proposed EAGNN algorithm.

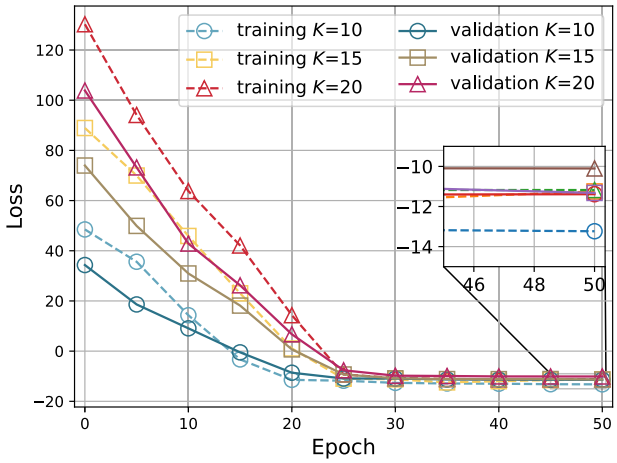

(a) Value of loss function.

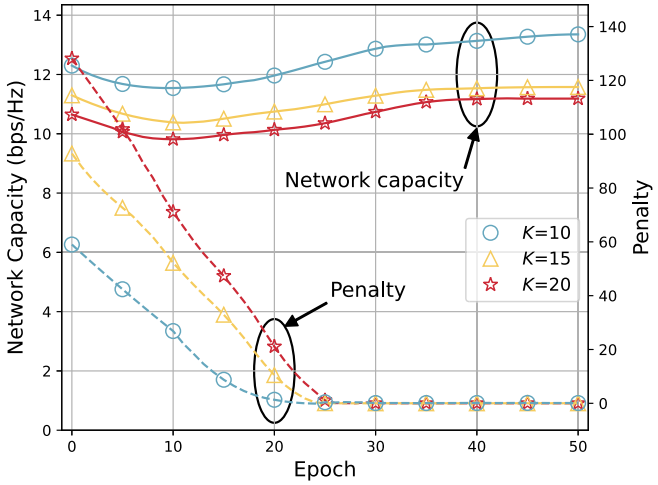

(b) Network capacity and penalty value.

Fig. 4. Convergence of EAGNN.

Fig. 5 shows the convergence performance of different algorithms on validation dataset. We can see that our proposed EAGNN and other benchmark algorithms achieve the convergence after a limited number of epochs. Furthermore, it is observed that EAGNN achieves the convergence faster than MLP and HetGNN algorithms. Meanwhile, the performance of EAGNN after the convergence is close to that of SCA-based algorithm. These results demonstrate the advantage of our proposed EAGNN on terms of training efficiency and optimality. This is because that two-stage structure of EAGNN improves the training efficiency to ensure the convergence and enhances global feature extraction to maximize network capacity.

B. Impact of Network Scale on Network Capacity

Fig. 6 shows network capacity of different algorithms versus K. We can observe that the network capacity obtained by different algorithms first increases and then decreases with the growth of K. This is because that numerous

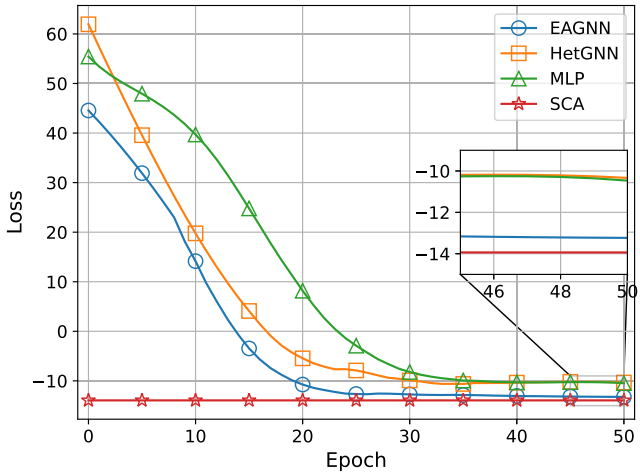

Fig. 5. Convergence of different algorithms.

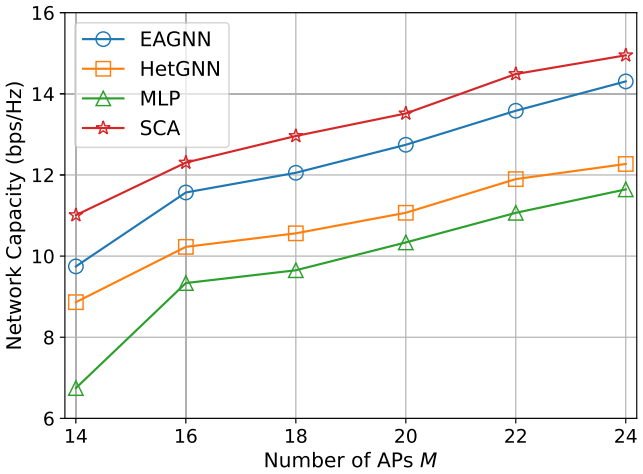

Fig. 7. Network capacity versus the number of APs M.

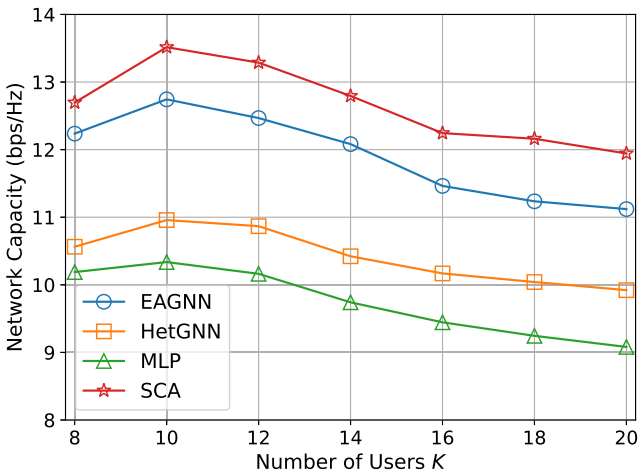

Fig. 6. Network capacity versus the number of user K.

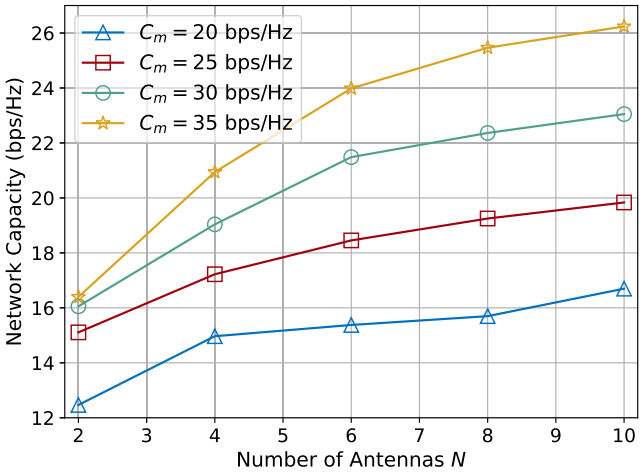

Fig. 8. Network capacity versus the number of AP antennas N with different fronthaul capacities.

users aggravate interference to degrade network capacity. Furthermore, it can be seen that although the degradation of network capacity exists, our proposed EAGNN algorithm achieves higher network capacity than HetGNN and MLP. The performance of EAGNN approximates to that of SCA-based algorithm which can acquire the near-optimal power control solution and however is with much higher computational complexity than EAGNN.

Fig. 7 shows network capacity of different algorithms versus M. We can see that the network capacity increases with the growth of M. This is because the growth of M can enhance cooperative gain among APs and heighten channel quality of cell-free downlink transmissions. Furthermore, it can be seen that our proposed EAGNN algorithm achieves higher network capacity than traditional MLP and HetGNN algorithms meanwhile approaches to the optimal solution with higher computational efficiency compared with SCA-based algorithm. This is because the designed message passing mechanism of EAGNN such as edge attention values and feature aggregations can effectively gather global information of considered heterogeneous network and extract corresponding relationships of interference and transmission links.

Fig. 8 shows network capacity versus N under different fronthaul capacities, i.e., the values of C_m. We can observe that the network capacity increases with the growth of N. This is because the growth of N can directly promote the gain of conjugate beamforming that is helpful to restrain co-channel interference and compensate channel fading. Moreover, it can be seen that the increase of fronthaul capacity leads to the growth of network capacity, since an enlarged C_m effectively reduces compression quantization noise power and strengthens the SINRs of cell-free downlink transmissions.

Fig. 9 shows the cumulative probability of all users' link transmission rates. It can be seen that our proposed EAGNN algorithm facilitates over 40% of users with at least 3 bps/Hz of achievable rate meanwhile ensures all the users to successfully access to cell-free and D2D heterogeneous network. The result demonstrates that EAGNN can achieve a better tradeoff between network capacity and users' achievable rates than MLP and HetGNN algorithms.

C. Generalization to Network Scenarios

Tables II and III show the generalization of different algorithms to network scenarios varying with M and K,

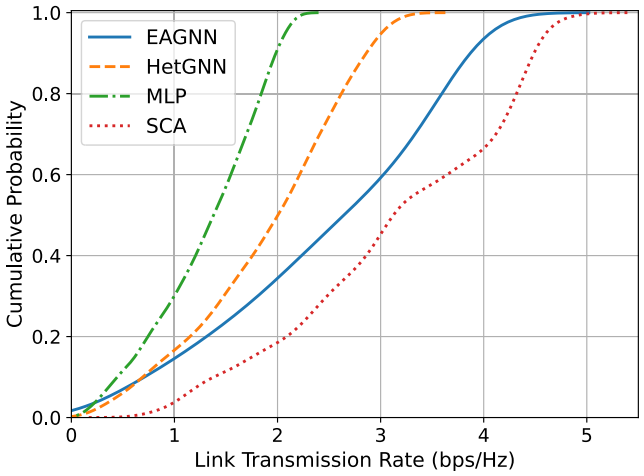

Fig. 9. Cumulative probability of all users' link transmission rates.

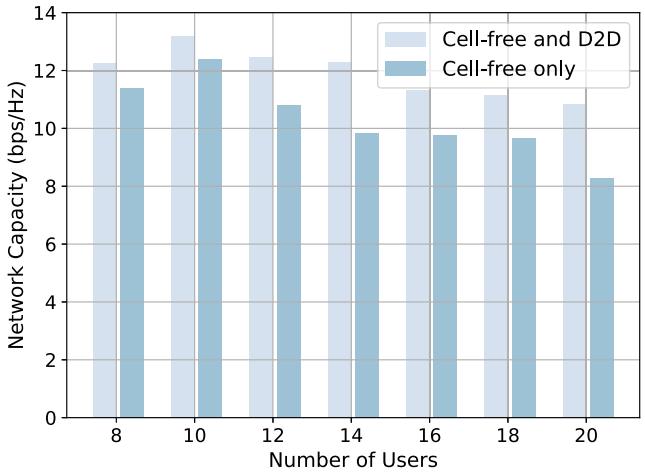

Fig. 10. Network capacity versus the number of user K in different network scenarios.

TABLE II
GENERALIZATION TO DIFFERENT VALUES OF M

Algorithms	$M = 16$	$M = 20$	$M = 24$
EAGNN	11.350 bps/Hz	12.744 bps/Hz	14.236 bps/Hz
EAGNN-retrained	11.568 bps/Hz	12.744 bps/Hz	14.306 bps/Hz
HetGNN-retrained	10.228 bps/Hz	10.958 bps/Hz	12.271 bps/Hz
MLP-retrained	9.335 bps/Hz	10.337 bps/Hz	11.644 bps/Hz

TABLE III
GENERALIZATION TO DIFFERENT VALUES OF K

Algorithms	$K = 10$	$K = 13$	$K = 16$
EAGNN	13.203 bps/Hz	12.286 bps/Hz	10.961 bps/Hz
EAGNN-retrained	13.203 bps/Hz	12.339 bps/Hz	11.320 bps/Hz
HetGNN-retrained	10.958 bps/Hz	10.847 bps/Hz	9.704 bps/Hz
MLP-retrained	10.337 bps/Hz	10.326 bps/Hz	9.445 bps/Hz

respectively. In this simulation experiment, EAGNN is trained within default simulation parameters and implemented in network scenarios with different values of M and K, while other algorithms are retrained in each network scenario. It can be seen that our proposed EAGNN algorithm is applicable for network capacity maximization even though M and K varies after it is trained in the scenario with default simulation parameter. Furthermore, the achieved network capacity by EAGNN without retraining is higher than that by HetGNN-retrained and MLP-retrained, and is close to that by EAGNN-retrained. Specifically, we can see that the performance gap between EAGNN and EAGNN-retrain is only 0.5-3%, which is very limited. This is thanks to permutation invariance and equivariance of EAGNN model.

Fig. 10 shows network capacity versus K in different network scenarios. We can observe that compared to cell-free RAN, cell-free and D2D heterogeneous networks can effectively increase network capacity. This demonstrates that D2D communications take the advantage of proximity transmission to mitigate traffic load of cell-free RAN and improve spectrum efficiency. This is because the establishment of D2D links relieves the pressure of fronthaul links to decrease compression quantization noise power and promote the utilization of fronthaul capacity and radio spectrum resource. Furthermore, it can be seen that our proposed EAGNN algorithm effectively coordinates interference among cell-free downlink transmissions and D2D communications to release the potential advantage of cell-free and D2D heterogeneous networks on network capacity.

V. CONCLUSION

In this paper, we have investigated interference coordination problem in cell-free and D2D heterogeneous networks to maximize network capacity. To tackle this problem, we have derived closed-form expressions for achievable rates of cell-free downlink transmissions and D2D communications, and then represented the relationships of all APs, DHs, and users as a heterogeneous graph. After that, we have proposed the EAGNN algorithm where its first stage exploits edge attention mechanism to optimize access mode selection and its second stage employs edge message passing to determine power control. Simulation results have shown that our proposed EAGNN algorithm can increase network capacity compared to traditional GNN and neural network based L2O methods, and approach the performance of advanced optimization method. Furthermore, our proposed EAGNN algorithm has exhibited well scalability and generalization to varying network scales and scenarios. Future works will focus on user-centric cell-free RAN with D2D in which GNN-based user association needs to be developed.

APPENDIX

A. Proof of Proposition 1

The detailed expression of received signal y_k^{c} at user k in (10) is given by

$$y_k = \sqrt{\rho^{\mathrm{c}}}\Big(1 - \sum_{i=1}^{I} \alpha_{i,k}\Big) \sum_{m=1}^{M} \sqrt{\eta_{m,k}^{\mathrm{c}}}\boldsymbol{g}_{m,k}^{\mathrm{T}}\hat{\boldsymbol{g}}_{m,k}^{*} s_k + \sqrt{\rho^{\mathrm{c}}} \sum_{m=1}^{M} \boldsymbol{g}_{m,k}^{\mathrm{T}} \sum_{k' \in \mathcal{K}\setminus k} \Big(1 - \sum_{i=1}^{I} \alpha_{i,k'}\Big) \sqrt{\eta_{m,k'}^{\mathrm{c}}}\hat{\boldsymbol{g}}_{m,k'}^{*} s_{k'}$$

$$+\sqrt{\rho^{\mathrm{c}}}\sum_{m=1}^{M}\boldsymbol{g}_{m,k}^{\mathrm{T}}\sum_{k'=1}^{K}\big(1-\sum_{i=1}^{I}\alpha_{i,k'}\big)\sqrt{\eta_{m,k'}^{\mathrm{c}}}\hat{\boldsymbol{g}}_{m,k'}^{*}q_{m,k'}+\sqrt{\rho^{\mathrm{d}}}\sum_{i=1}^{I}G_{i,k}\sum_{k'=1}^{K}\alpha_{i,k'}\sqrt{\eta_{i,k'}^{\mathrm{d}}}s_{k'}+n_{k}^{\mathrm{u}},\tag{33}$$

which can be rewritten as

$$y_{k}^{\mathrm{c}}=\mathrm{CS}_{k}\cdot s_{k}+\mathrm{BU}_{k}\cdot s_{k}+\sum_{k'\in\mathcal{K}\setminus k}\mathrm{CI}_{k,k'}\cdot s_{k'}+\sum_{k'=1}^{K}\mathrm{QN}_{k,k'}\cdot q_{m,k'}+\sum_{k'=1}^{K}\mathrm{DI}_{k,k'}\cdot s_{k'}+n_{k}^{\mathrm{u}}.\tag{34}$$

CS_k, BU_k, $\mathrm{CI}_{k,k'}$, $\mathrm{DI}_{k,k'}$, and $\mathrm{QN}_{k,k'}$ represent the strength of desired signal, the beamforming gain uncertainty, interference from other downlink transmissions, interference from D2D communications, and the strength of quantization noise, respectively. The achievable rate of downlink transmission for user k is given by (35), shown at the bottom of the page, where $\mathbb{E}\left\{|n_{k}^{\mathrm{u}}|^{2}\right\}=1$ [12].

First, we compute the term of CS_k. Let $\tilde{\boldsymbol{g}}_{m,k}=\boldsymbol{g}_{m,k}-\hat{\boldsymbol{g}}_{m,k}$ denote the channel estimation error, where each element follows the distribution $\mathcal{CN}\big(0,u_{m,k}-\frac{\gamma_{m,k}^{\mathrm{c}}}{N}\big)$. Due to the properties of MMSE estimation, $\tilde{\boldsymbol{g}}_{m,k}$ and $\hat{\boldsymbol{g}}_{m,k}$ are independent of each other. Thus, we can get

$$\begin{aligned}\mathrm{CS}_{k}&=\sqrt{\rho^{\mathrm{c}}}\big(1-\sum_{i=1}^{I}\alpha_{i,k}\big)\sum_{m=1}^{M}\sqrt{\eta_{m,k}^{\mathrm{c}}}\mathbb{E}\big\{\big(\hat{\boldsymbol{g}}_{m,k}^{\mathrm{T}}+\tilde{\boldsymbol{g}}_{m,k}^{\mathrm{T}}\big)\hat{\boldsymbol{g}}_{m,k}^{*}\big\}\\&=\sqrt{\rho^{\mathrm{c}}}\big(1-\sum_{i=1}^{I}\alpha_{i,k}\big)\sum_{m=1}^{M}\sqrt{\eta_{m,k}^{\mathrm{c}}}\mathbb{E}\big\{\hat{\boldsymbol{g}}_{m,k}^{\mathrm{T}}\hat{\boldsymbol{g}}_{m,k}^{*}\big\}\\&=\sqrt{\rho^{\mathrm{c}}}\big(1-\sum_{i=1}^{I}\alpha_{i,k}\big)\sum_{m=1}^{M}\sqrt{\eta_{m,k}^{\mathrm{c}}}\gamma_{m,k}^{\mathrm{c}}.\end{aligned}\tag{36}$$

Second, we compute the term of $\mathbb{E}\left\{|\mathrm{BU}_k|^2\right\}$, where $\mathrm{BU}_k=\sqrt{\rho^{\mathrm{c}}}\big(1-\sum_{i=1}^{I}\alpha_{i,k}\big)\big(\sum_{m=1}^{M}\sqrt{\eta_{m,k}^{\mathrm{c}}}\boldsymbol{g}_{m,k}^{\mathrm{T}}\hat{\boldsymbol{g}}_{m,k}^{*}-\mathbb{E}\{\sum_{m=1}^{M}\sqrt{\eta_{m,k}^{\mathrm{c}}}\boldsymbol{g}_{m,k}^{\mathrm{T}}\hat{\boldsymbol{g}}_{m,k}^{*}\}\big)$. Hence, we can get

$$\mathbb{E}\big\{|\mathrm{BU}_{k}|^{2}\big\}=\rho^{\mathrm{c}}\big(1-\sum_{i=1}^{I}\alpha_{i,k}\big)\sum_{m=1}^{M}\eta_{m,k}^{\mathrm{c}}\mathbb{E}\big\{\big|\tilde{\mathrm{BU}}_{k}\big|^{2}\big\},\tag{37}$$

$$\begin{aligned}\mathbb{E}\big\{\big|\tilde{\mathrm{BU}}_{k}\big|^{2}\big\}&=\mathbb{E}\big\{\big|\boldsymbol{g}_{m,k}^{\mathrm{T}}\hat{\boldsymbol{g}}_{m,k}^{*}\big|^{2}\big\}-\big|\mathbb{E}\{\boldsymbol{g}_{m,k}^{\mathrm{T}}\hat{\boldsymbol{g}}_{m,k}^{*}\}\big|^{2}\\&=\mathbb{E}\big\{\big|\tilde{\boldsymbol{g}}_{m,k}^{\mathrm{T}}\hat{\boldsymbol{g}}_{m,k}^{*}\big|^{2}\big\}+\mathbb{E}\big\{\big|\hat{\boldsymbol{g}}_{m,k}\big|^{4}\big\}-\big(\gamma_{m,k}^{\mathrm{c}}\big)^{2}\\&\overset{(a)}{=}\big(u_{m,k}-\frac{\gamma_{m,k}^{\mathrm{c}}}{N}\big)\gamma_{m,k}^{\mathrm{c}}+\big(1+\frac{1}{N}\big)\big(\gamma_{m,k}^{\mathrm{c}}\big)^{2}-\big(\gamma_{m,k}^{\mathrm{c}}\big)^{2}\\&=\gamma_{m,k}^{\mathrm{c}}u_{m,k},\end{aligned}\tag{38}$$

where (a) is due to $\mathbb{E}\big\{\big|\tilde{\boldsymbol{g}}_{m,k}\big|^{2}\big\}=u_{m,k}-\frac{\gamma_{m,k}^{\mathrm{c}}}{N}$ and $\mathbb{E}\big\{\big|\hat{\boldsymbol{g}}_{m,k}\big|^{4}\big\}=\big(1+\frac{1}{N}\big)\big(\gamma_{m,k}^{\mathrm{c}}\big)^{2}$ [27].

Third, we compute $\mathbb{E}\left\{\left|\mathrm{CI}_{k,k'}\right|^{2}\right\}$ and $\mathbb{E}\big\{\big|\mathrm{QN}_{k,k'}q_{m,k'}\big|^{2}\big\}$ based on (36) and (37). Following the hints provided in [12], it can be obtained that

$$\mathbb{E}\big\{\big|\mathrm{CI}_{k,k'}\big|^{2}\big\}=\rho^{\mathrm{c}}\big(1-\sum_{i=1}^{I}\alpha_{i,k'}\big)\mathbb{E}\big\{\big|\tilde{\mathrm{CI}}_{k,k'}\big|^{2}\big\}.\tag{39}$$

$$\begin{aligned}\mathbb{E}\big\{\big|\tilde{\mathrm{CI}}_{k,k'}\big|^{2}\big\}&=\mathbb{E}\big\{\big|\sum_{m=1}^{M}\sqrt{\eta_{m,k'}^{\mathrm{c}}}\boldsymbol{g}_{m,k}^{\mathrm{T}}\hat{\boldsymbol{g}}_{m,k'}^{*}\big|^{2}\big\}\\&=\big|\phi_{k'}^{\mathrm{H}}\phi_{k}\big|^{2}\big(\sum_{m=1}^{M}\sqrt{\eta_{m,k'}^{\mathrm{c}}}\gamma_{m,k'}^{\mathrm{c}}\frac{u_{m,k}}{u_{m,k'}}\big)^{2}+\sum_{m=1}^{M}\eta_{m,k'}^{\mathrm{c}}u_{m,k}\gamma_{m,k'}^{\mathrm{c}}.\end{aligned}\tag{40}$$

Similarly, we can get that

$$\begin{aligned}&\mathbb{E}\big\{\big|\mathrm{QN}_{k,k'}q_{m,k'}\big|^{2}\big\}\\&=\rho^{\mathrm{c}}\big(1-\sum_{i=1}^{I}\alpha_{i,k'}\big)\Big[\big|\phi_{k'}^{\mathrm{H}}\phi_{k}\big|^{2}\big(\sum_{m=1}^{M}\sqrt{\eta_{m,k'}^{\mathrm{c}}}\gamma_{m,k'}^{\mathrm{c}}\frac{u_{m,k}}{u_{m,k'}}\big)^{2}+\sum_{m=1}^{M}\eta_{m,k'}^{\mathrm{c}}u_{m,k}\gamma_{m,k'}^{\mathrm{c}}\Big]Q_{m,k'}.\end{aligned}\tag{41}$$

Finally, we compute $\mathbb{E}\big\{\big|\mathrm{DI}_{k,k'}\big|^{2}\big\}$ which is given by

$$\begin{aligned}\mathbb{E}\left\{\left|\mathrm{DI}_{k,k'}\right|^{2}\right\}&=\rho^{\mathrm{d}}\sum_{i=1}^{I}\alpha_{i,k'}\eta_{i,k'}^{\mathrm{d}}\mathbb{E}\big\{\big|G_{i,k}\big|^{2}\big\}\\&=\rho^{\mathrm{d}}\sum_{i=1}^{I}\alpha_{i,k'}\eta_{i,k'}^{\mathrm{d}}v_{i,k}.\end{aligned}\tag{42}$$

Consequently, we substitute (36)-(42) into (35) to obtain (11).

B. Proof of Proposition 2

The received signal y_k can be rewritten as

$$\begin{aligned}y_{k}^{\mathrm{d}}&=\sqrt{\rho^{\mathrm{d}}}\sum_{i=1}^{I}\alpha_{i,k}\sqrt{\eta_{i,k}^{\mathrm{d}}}(\hat{G}_{i,k}+\tilde{G}_{i,k})s_{k}\\&+\sqrt{\rho^{\mathrm{c}}}\sum_{m=1}^{M}\sum_{k'=1}^{K}\big(1-\sum_{i=1}^{I}\alpha_{i,k'}\big)\sqrt{\eta_{m,k'}^{\mathrm{c}}}\boldsymbol{g}_{m,k}^{\mathrm{T}}\hat{\boldsymbol{g}}_{m,k'}^{*}s_{k'}\\&+\sqrt{\rho^{\mathrm{c}}}\sum_{m=1}^{M}\sum_{k'=1}^{K}\big(1-\sum_{i=1}^{I}\alpha_{i,k'}\big)\sqrt{\eta_{m,k'}^{\mathrm{c}}}\boldsymbol{g}_{m,k}^{\mathrm{T}}\hat{\boldsymbol{g}}_{m,k'}^{*}q_{m,k'}\\&+\sqrt{\rho^{\mathrm{d}}}\sum_{i=1}^{I}\sum_{k'\in\mathcal{K}\setminus k}\alpha_{i,k'}\sqrt{\eta_{i,k'}^{\mathrm{d}}}G_{i,k}s_{k'}+n_{k}^{\mathrm{u}}.\end{aligned}\tag{43}$$

where $\tilde{G}_{i,k}\sim\mathcal{CN}\big(0,v_{i,k}-\gamma_{i,k}^{\mathrm{d}}\big)$ denotes the channel estimation error for $G_{i,k}$. Similarly, the achievable rate of D2D

$$R_{k}^{\mathrm{c}}=\log_{2}\big(1+\frac{\big|\mathrm{CS}_{k}\big|^{2}}{\mathbb{E}\big\{\big|\mathrm{BU}_{k}\big|^{2}\big\}+\sum_{k'\in\mathcal{K}\setminus k}\mathbb{E}\big\{\big|\mathrm{CI}_{k,k'}\big|^{2}\big\}+\sum_{k'=1}^{K}\mathbb{E}\big\{\big|\mathrm{QN}_{k,k'}q_{m,k'}\big|^{2}\big\}+\sum_{k'=1}^{K}\mathbb{E}\big\{\big|\mathrm{DI}_{k,k'}\big|^{2}\big\}+1}\big).\tag{35}$$

$$R_k^{\mathrm{d}} = \log_2\big(1 + \frac{\left|\mathrm{DS}_k\right|^2}{\sum_{k'=1}^{K}\mathbb{E}\{\left|\mathrm{CI}_{k,k'}\right|^2\} + \sum_{k'=1}^{K}\mathbb{E}\{\left|\mathrm{QN}_{k,k'}q_{m,k'}\right|^2\} + \sum_{k'\in\mathcal{K}\setminus k}\mathbb{E}\{\left|\mathrm{DI}_{k,k'}\right|^2\} + 1}\big). \tag{44}$$

communication for user k is given by (44), shown at the top of the page, in which the strength of its desired signal is $\left|\mathrm{DS}_k\right|^2$.

Now, we compute DS_k and can obtain that

$$\begin{aligned}\left|\mathrm{DS}_k\right|^2 &= \rho^{\mathrm{d}}\sum_{i=1}^{I}\alpha_{i,k}\eta_{i,k}^{\mathrm{d}}\mathbb{E}\{\left|\hat{G}_{i,k}+\tilde{G}_{i,k}\right|^2\}\\ &= \rho^{\mathrm{d}}\sum_{i=1}^{I}\alpha_{i,k}\eta_{i,k}^{\mathrm{d}}\big(\mathbb{E}\{\left|\hat{G}_{i,k}\right|^2\}+\mathbb{E}\{\left|\tilde{G}_{i,k}\right|^2\}\big)\\ &\overset{(b)}{=} \rho^{\mathrm{d}}\sum_{i=1}^{I}\alpha_{i,k}\eta_{i,k}^{\mathrm{d}}v_{i,k}\end{aligned} \tag{45}$$

where (b) is due to $\mathbb{E}\{\left|\hat{G}_{i,k}\right|^2\} = \gamma_{i,k}^{\mathrm{d}} = \sqrt{\tau_{\mathrm{p}}\rho_{\mathrm{p}}}v_{i,k}c_{i,k}^{\mathrm{d}}$ and $\mathbb{E}\{\left|\tilde{G}_{i,k}\right|^2\} = v_{i,k} - \gamma_{i,k}^{\mathrm{d}}$. Then, we substitute (39)-(42) and (45) into (44) to obtain (15).

C. Proof of Proposition 3

For a permutation operator π, it can generate a permutation of $\mathcal{N}\left(v_k^{\mathrm{UE}}\right)$, i.e., $\mathcal{N}\left(v_{\pi(k)}^{\mathrm{UE}}\right) = \{v_{\pi(j)}, v_j \in \mathcal{N}\left(v_k^{\mathrm{UE}}\right)\}$. By means of the mean pooling, we can get the aggregated vertex feature of $\mathcal{N}\left(v_{\pi(k)}^{\mathrm{UE}}\right)$ as

$$\boldsymbol{\Omega}_{\pi(k)}^{\mathrm{UE},(t)} = \frac{1}{\left|\mathcal{N}\left(v_{\pi(k)}^{\mathrm{UE}}\right)\right|}\sum_{v_{\pi(j)}\in\mathcal{N}\left(v_{\pi(k)}^{\mathrm{UE}}\right)} a_{\pi(j),k}\boldsymbol{W}_1^{(t)}\boldsymbol{\zeta}_{\pi(j),k}, \tag{46}$$

$$\triangleq \frac{1}{\left|\mathcal{N}\left(v_k^{\mathrm{UE}}\right)\right|}\sum_{v_j\in\mathcal{N}\left(v_k^{\mathrm{UE}}\right)} a_{j,k}\boldsymbol{W}_1^{(t)}\boldsymbol{\zeta}_{j,k} = \boldsymbol{\Omega}_k^{\mathrm{UE},(t)}. \tag{47}$$

where $\triangleq$ is due to $\left|\mathcal{N}\left(v_{\pi(k)}^{\mathrm{UE}}\right)\right| = \left|\mathcal{N}\left(v_k^{\mathrm{UE}}\right)\right|$ and the unchanged summation result. Therefore, π cannot change the results of vertex feature aggregation. Now, we finish the proof of Proposition 3.

D. Proof of Proposition 4

We first consider the first stage of EAGNN for access mode selection, denoted by $\mathrm{EAGNN}_1(\cdot)$. Given a permutation π, we have initial conditions that are $\mathbf{z}_{\pi(k)}^{\mathrm{UE},(0)} = \mathbf{z}_k^{\mathrm{UE},(0)}$, $\mathcal{N}\left(v_{\pi(k)}^{\mathrm{UE}}\right) = \mathcal{N}\left(v_k^{\mathrm{UE}}\right)$, and $\boldsymbol{\zeta}_{\pi(j),\pi(k)} = \boldsymbol{\zeta}_{j,k}$ for vertex v_k^{UE}. In order to prove $\mathbf{z}_{\pi(k)}^{\mathrm{UE},(T_1)} = \mathbf{z}_k^{\mathrm{UE},(T_1)}$, we utilize the induction and assume that the base case of $t=0$ follows initial conditions and $\mathbf{z}_{\pi(k)}^{\mathrm{UE},(\tau-1)} = \mathbf{z}_k^{\mathrm{UE},(\tau-1)}$ when $t=\tau-1$. Then, vertex features of v_k^{UE} and $v_{\pi(k)}^{\mathrm{UE}}$ at layer τ are updated as

$$\mathbf{z}_k^{\mathrm{UE},(\tau)} = \boldsymbol{W}_2^{(\tau)}\boldsymbol{\Omega}_k^{\mathrm{UE},(\tau)} + \mathbf{z}_k^{\mathrm{UE},(\tau-1)}, \tag{48}$$

$$\mathbf{z}_{\pi(k)}^{\mathrm{UE},(\tau)} = \boldsymbol{W}_2^{(\tau)}\boldsymbol{\Omega}_{\pi(k)}^{\mathrm{UE},(\tau)} + \mathbf{z}_{\pi(k)}^{\mathrm{UE},(\tau-1)}. \tag{49}$$

Following induction assumption and initial conditions, we can get $\boldsymbol{\Omega}_k^{\mathrm{UE},(\tau)} = \boldsymbol{\Omega}_{\pi(k)}^{\mathrm{UE},(\tau)}$ and $\mathbf{z}_k^{\mathrm{UE},(\tau-1)} = \mathbf{z}_{\pi(k)}^{\mathrm{UE},(\tau-1)}$ such that $\mathbf{z}_{\pi(k)}^{\mathrm{UE},(\tau)} = \mathbf{z}_k^{\mathrm{UE},(\tau)}$ is obtained. Thus, we have $\mathbf{z}_{\pi(k)}^{\mathrm{UE},(T_1)} = \mathbf{z}_k^{\mathrm{UE},(T_1)}$ for a T_1-layer first stage of EAGNN. At the layer T_1, we can get $\bar{\zeta}_{\pi(i),\pi(k)}^{\mathrm{DH}} = \bar{\zeta}_{i,k}^{\mathrm{DH}}$. Accordingly, $\mathrm{EAGNN}_1(\cdot)$ has the permutation equivariance property, i.e., $\mathrm{EAGNN}_1(\pi\star\mathbf{Z}, \pi\star\mathbf{E}) = \pi\star\mathrm{EAGNN}_1(\mathbf{Z},\mathbf{E})$.

Second, we consider the second stage of EAGNN for power control, denoted by $\mathrm{EAGNN}_2(\cdot)$. Given a permutation π, we have initial conditions that are $\mathbf{z}_{\pi(m)}^{\mathrm{AP},(0)} = \mathbf{z}_m^{\mathrm{AP},(0)}$ and $\mathbf{z}_{\pi(i)}^{\mathrm{DH},(0)} = \mathbf{z}_i^{\mathrm{DH},(0)}$, $\mathcal{N}\left(v_{\pi(m)}^{\mathrm{AP}}\right) = \mathcal{N}\left(v_m^{\mathrm{AP}}\right)$ and $\mathcal{N}\left(v_{\pi(i)}^{\mathrm{DH}}\right) = \mathcal{N}\left(v_i^{\mathrm{DH}}\right)$, $\zeta_{\pi(m),\pi(k)}^{\mathrm{AP}} = \zeta_{m,k}^{\mathrm{AP}}$ and $\zeta_{\pi(i),\pi(k)}^{\mathrm{DH}} = \zeta_{i,k}^{\mathrm{DH}}$, for vertices v_m^{AP} and v_i^{DH}, respectively. Similarly, we utilize the induction and assume that the base case of $t=0$ follows initial conditions meanwhile $\mathbf{z}_{\pi(m)}^{\mathrm{AP},(\tau-1)} = \mathbf{z}_m^{\mathrm{AP},(\tau-1)}$ and $\mathbf{z}_{\pi(i)}^{\mathrm{DH},(\tau-1)} = \mathbf{z}_i^{\mathrm{DH},(\tau-1)}$ when $t=\tau-1$. After that, vertex features at layer τ are updated as

$$\mathbf{z}_m^{\mathrm{AP},(\tau)} = \boldsymbol{W}_2^{(\tau)}\boldsymbol{\Omega}_m^{\mathrm{AP},(\tau)} + \mathbf{z}_m^{\mathrm{AP},(\tau-1)}, \tag{50}$$

$$\mathbf{z}_{\pi(m)}^{\mathrm{AP},(\tau)} = \boldsymbol{W}_2^{(\tau)}\boldsymbol{\Omega}_{\pi(m)}^{\mathrm{AP},(\tau)} + \mathbf{z}_{\pi(m)}^{\mathrm{AP},(\tau-1)}, \tag{51}$$

$$\mathbf{z}_i^{\mathrm{DH},(\tau)} = \boldsymbol{W}_2^{(\tau)}\boldsymbol{\Omega}_i^{\mathrm{DH},(\tau)} + \mathbf{z}_i^{\mathrm{DH},(\tau-1)}, \tag{52}$$

$$\mathbf{z}_{\pi(i)}^{\mathrm{DH},(\tau)} = \boldsymbol{W}_2^{(\tau)}\boldsymbol{\Omega}_{\pi(i)}^{\mathrm{DH},(\tau)} + \mathbf{z}_{\pi(i)}^{\mathrm{DH},(\tau-1)}. \tag{53}$$

Following induction assumption and initial conditions, we have $\boldsymbol{\Omega}_{\pi(m)}^{\mathrm{AP},(\tau)} = \boldsymbol{\Omega}_m^{\mathrm{AP},(\tau)}$ and $\boldsymbol{\Omega}_{\pi(i)}^{\mathrm{DH},(\tau)} = \boldsymbol{\Omega}_i^{\mathrm{DH},(\tau)}$, $\mathbf{z}_{\pi(m)}^{\mathrm{AP},(\tau-1)} = \mathbf{z}_m^{\mathrm{AP},(\tau-1)}$ and $\mathbf{z}_{\pi(i)}^{\mathrm{DH},(\tau-1)} = \mathbf{z}_i^{\mathrm{DH},(\tau-1)}$ such that $\mathbf{z}_{\pi(m)}^{\mathrm{AP},(\tau)} = \mathbf{z}_m^{\mathrm{AP},(\tau)}$ and $\mathbf{z}_{\pi(i)}^{\mathrm{DH},(\tau)} = \mathbf{z}_i^{\mathrm{DH},(\tau)}$. Hence, we can get $\mathbf{z}_{\pi(m)}^{\mathrm{AP},(T_2)} = \mathbf{z}_m^{\mathrm{AP},(T_2)}$ and $\mathbf{z}_{\pi(i)}^{\mathrm{DH},(T_2)} = \mathbf{z}_i^{\mathrm{DH},(T_2)}$ for a T_2-layer second stage of EAGNN. At the layer T_2, we can obtain $\hat{\zeta}_{\pi(m),\pi(k)}^{\mathrm{AP}} = \hat{\zeta}_{m,k}^{\mathrm{AP}}$ and $\hat{\zeta}_{\pi(i),\pi(k)}^{\mathrm{DH}} = \hat{\zeta}_{i,k}^{\mathrm{DH}}$. Consequently, $\mathrm{EAGNN}_2(\cdot)$ has the permutation equivariance property, i.e., $\mathrm{EAGNN}_2(\pi\star\mathbf{Z}, \pi\star\mathbf{E}) = \pi\star\mathrm{EAGNN}_2(\mathbf{Z},\mathbf{E})$.

Now, we finish the proof of Proposition 4.

REFERENCES

[1] E. Björnson and L. Sanguinetti, "Making cell-free massive MIMO competitive with MMSE processing and centralized implementation," *IEEE Trans. Wireless Commun.*, vol. 19, no. 1, pp. 77–90, Jan. 2020.

[2] Y. Zhang et al., "Beyond cell-free MIMO: Energy efficient reconfigurable intelligent surface aided cell-free MIMO communications," *IEEE Trans. Cognit. Commun. Netw.*, vol. 7, no. 2, pp. 412–426, Jun. 2021.

[3] M. Ke, Z. Gao, Y. Wu, X. Gao, and K.-K. Wong, "Massive access in cell-free massive MIMO-based Internet of Things: Cloud computing and edge computing paradigms," *IEEE J. Sel. Areas Commun.*, vol. 39, no. 3, pp. 756–772, Mar. 2021.

[4] B. Lyu, C. Zhou, S. Gong, W. Wu, D. T. Hoang, and D. Niyato, "Energy-efficiency maximization for STAR-RIS enabled cell-free symbiotic radio communications," *IEEE Trans. Cognit. Commun. Netw.*, vol. 10, no. 6, pp. 2209–2223, Dec. 2024.

[5] Y. Yuan, T. Yang, Y. Hu, H. Feng, and B. Hu, "Two-timescale resource allocation for cooperative D2D communication: A matching game approach," *IEEE Trans. Veh. Technol.*, vol. 70, no. 1, pp. 543–557, Jan. 2021.

[6] M. Feng, S. Mao, and T. Jiang, "Dealing with link blockage in mmWave networks: A combination of D2D relaying, multi-beam reflection, and handover," *IEEE Trans. Wireless Commun.*, vol. 21, no. 8, pp. 6746–6759, Aug. 2022.

[7] F. Fredj, Y. Al-Eryani, S. Maghsudi, M. Akrout, and E. Hossain, "Distributed beamforming techniques for cell-free wireless networks using deep reinforcement learning," *IEEE Trans. Cognit. Commun. Netw.*, vol. 8, no. 2, pp. 1186–1201, Jun. 2022.

[8] S. Feng, X. Lu, K. Zhu, D. Niyato, and P. Wang, "Covert D2D communication underlaying cellular network: A system-level security perspective," *IEEE Trans. Wireless Commun.*, vol. 23, no. 8, pp. 9518–9533, Aug. 2024.

[9] X. Wang et al., "RadioDiff: An effective generative diffusion model for sampling-free dynamic radio map construction," *IEEE Trans. Cognit. Commun. Netw.*, vol. 11, no. 2, pp. 738–750, Apr. 2025.

[10] T. Jiang, M. Jin, Q. Guo, Y. Liu, Y. Li, and J. Yao, "Full-duplex ISAC-enabled D2D underlaid cellular networks: Joint transceiver beamforming and power allocation," *IEEE Trans. Cognit. Commun. Netw.*, early access, Mar. 18, 2025, doi: 10.1109/TCCN.2025.3552627.

[11] D. Yan, Y. Dai, L. Lyu, and N. Cheng, "Edge-featured graph attention network for power control in cell-free and D2D heterogeneous networks," in *Proc. 16th Int. Conf. Wireless Commun. Signal Process. (WCSP)*, Oct. 2024, pp. 678–683.

[12] H. Q. Ngo, A. Ashikhmin, H. Yang, E. G. Larsson, and T. L. Marzetta, "Cell-free massive MIMO versus small cells," *IEEE Trans. Wireless Commun.*, vol. 16, no. 3, pp. 1834–1850, Mar. 2017.

[13] W.-K. Lai, Y.-C. Wang, H.-C. Lin, and J.-W. Li, "Efficient resource allocation and power control for LTE—A D2D communication with pure D2D model," *IEEE Trans. Veh. Technol.*, vol. 69, no. 3, pp. 3202–3216, Mar. 2020.

[14] M. Xu et al., "Unleashing the power of edge-cloud generative AI in mobile networks: A survey of AIGC services," *IEEE Commun. Surveys Tuts.*, vol. 26, no. 2, pp. 1127–1170, Jan. 2024.

[15] N. Cheng et al., "Mixture of gradient: A unified enhancing approach for deep-learning-based wireless network optimization," *IEEE Internet Things J.*, vol. 12, no. 13, pp. 25487–25499, Jul. 2025.

[16] Y. Dai et al., "A survey of graph-based resource management in wireless networks—Part I: Optimization approaches," *IEEE Trans. Cognit. Commun. Netw.*, vol. 11, no. 4, pp. 2078–2100, Aug. 2025.

[17] Z. Wang, K. Huang, and Y. C. Eldar, "Spectrum breathing: Protecting over-the-air federated learning against interference," *IEEE Trans. Wireless Commun.*, vol. 23, no. 8, pp. 10058–10071, Aug. 2024.

[18] X. Li, M. Chen, Y. Liu, Z. Zhang, D. Liu, and S. Mao, "Graph neural networks for joint communication and sensing optimization in vehicular networks," *IEEE J. Sel. Areas Commun.*, vol. 41, no. 12, pp. 3893–3907, Dec. 2023.

[19] Y. Dai et al., "A survey of graph-based resource management in wireless networks—Part II: Learning approaches," *IEEE Trans. Cognit. Commun. Netw.*, vol. 11, no. 4, pp. 2101–2122, Aug. 2025.

[20] J. He et al., "Load-aware network resource orchestration in LEO satellite network: A GAT-based approach," *IEEE Internet Things J.*, vol. 11, no. 9, pp. 15969–15984, May 2024.

[21] Ö. T. Demir and E. Björnson, "Joint power control and LSFD for wireless-powered cell-free massive MIMO," *IEEE Trans. Wireless Commun.*, vol. 20, no. 3, pp. 1756–1769, Mar. 2021.

[22] T. C. Mai, H. Q. Ngo, and L.-N. Tran, "Energy efficiency maximization in large-scale cell-free massive MIMO: A projected gradient approach," *IEEE Trans. Wireless Commun.*, vol. 21, no. 8, pp. 6357–6371, Aug. 2022.

[23] J. Dai et al., "Two-timescale transmission design for RIS-aided cell-free massive MIMO systems," *IEEE Trans. Wireless Commun.*, vol. 23, no. 6, pp. 6498–6517, Jun. 2024.

[24] J. Fang, P. Zhu, J. Li, F.-C. Zheng, and X. You, "Cell-free mMIMO systems in short packet transmission regime: Pilot and power allocation," *IEEE Trans. Veh. Technol.*, vol. 73, no. 6, pp. 8322–8337, Jun. 2024.

[25] M. Hamdi, A. Ben Hamed, D. Yuan, and M. Zaied, "Energy-efficient joint task assignment and power control in energy-harvesting D2D offloading communications," *IEEE Internet Things J.*, vol. 9, no. 8, pp. 6018–6031, Apr. 2022.

[26] A. Ramezani-Kebrya, B. Liang, M. Dong, and G. Boudreau, "Robust design of multicell D2D communication under partial CSI," *IEEE Internet Things J.*, vol. 9, no. 3, pp. 2404–2418, Feb. 2022.

[27] X. Qiao, Y. Zhang, M. Zhou, L. Yang, and H. Zhu, "Downlink achievable rate of D2D underlaid cell-free massive MIMO systems with low-resolution DACs," *IEEE Syst. J.*, vol. 16, no. 3, pp. 3855–3866, Sep. 2022.

[28] H. Masoumi, M. J. Emadi, and S. Buzzi, "Coexistence of D2D communications and cell-free massive MIMO systems with low resolution ADC for improved throughput in beyond-5G networks," *IEEE Trans. Commun.*, vol. 70, no. 2, pp. 999–1013, Feb. 2022.

[29] Y. Shen, Y. Shi, J. Zhang, and K. B. Letaief, "Graph neural networks for scalable radio resource management: Architecture design and theoretical analysis," *IEEE J. Sel. Areas Commun.*, vol. 39, no. 1, pp. 101–115, Jan. 2021.

[30] J. Guo and C. Yang, "Learning power allocation for multi-cell-multi-user systems with heterogeneous graph neural networks," *IEEE Trans. Wireless Commun.*, vol. 21, no. 2, pp. 884–897, Feb. 2022.

[31] Y. Shen, J. Zhang, S. H. Song, and K. B. Letaief, "Graph neural networks for wireless communications: From theory to practice," *IEEE Trans. Wireless Commun.*, vol. 22, no. 5, pp. 3554–3569, May 2023.

[32] V.-C. Luu and J.-P. Hong, "GNN-based meta-learning approach for adaptive power control in dynamic D2D communications," *IEEE Trans. Veh. Technol.*, vol. 73, no. 4, pp. 5982–5987, Apr. 2024.

[33] X. Yan, Z. Wang, Y. Jia, Z. Zhang, and Y. Huang, "Access point selection and beamforming design for cell-free network: From fractional programming to GNN," *IEEE Trans. Wireless Commun.*, vol. 23, no. 8, pp. 9345–9360, Aug. 2024.

[34] G. Liu, H. Deng, X. Qian, W. Zhang, and H. Dong, "Joint pilot and data power control for cell-free massive MIMO IoT systems," *IEEE Sensors J.*, vol. 22, no. 24, pp. 24647–24657, Dec. 2022.

[35] P. Parida and H. S. Dhillon, "Cell-free massive MIMO with finite fronthaul capacity: A stochastic geometry perspective," *IEEE Trans. Wireless Commun.*, vol. 22, no. 3, pp. 1555–1572, Mar. 2023.

[36] S. Elhoushy and W. Hamouda, "Downlink performance of limited-fronthaul cell-free massive MIMO," in *Proc. IEEE Int. Conf. Commun.*, Jun. 2021, pp. 1–6.

[37] L. Lyu et al., "AGV-assisted adaptive cooperative transmission for state estimation in industrial IoT systems," *IEEE Trans. Veh. Technol.*, vol. 74, no. 2, pp. 2390–2405, Feb. 2025.

[38] Z. Wang, A. E. Kalør, Y. Zhou, P. Popovski, and K. Huang, "Ultra-low-latency edge inference for distributed sensing," *IEEE Trans. Wireless Commun.*, early access, Aug. 8, 2025, doi: 10.1109/TWC.2025.3593802.

[39] T. Jiang, H. V. Cheng, and W. Yu, "Learning to reflect and to beamform for intelligent reflecting surface with implicit channel estimation," *IEEE J. Sel. Areas Commun.*, vol. 39, no. 7, pp. 1931–1945, Jul. 2021.

[40] M. Wang et al., "Deep graph library: A graph-centric, highly-performant package for graph neural networks," 2019, *arXiv:1909.01315*.

[41] Z. Wang, Q. Zeng, H. Zheng, and K. Huang, "Revisiting outage for edge inference systems," 2025, *arXiv:2504.03686*.

[42] N. Rajapaksha, K. B. Shashika Manosha, N. Rajatheva, and M. Latva-Aho, "Deep learning-based power control for cell-free massive MIMO networks," in *Proc. IEEE Int. Conf. Commun.*, Jun. 2021, pp. 1–7.

[43] T. Lipp and S. Boyd, "Variations and extension of the convexconcave procedure," *Optim. Eng.*, vol. 17, Jun. 2016, Art. no. 263287.

Yanpeng Dai (Member, IEEE) received the B.Eng. degree in telecommunication engineering from Shandong Normal University, Jinan, Shandong, China, in 2014, and the Ph.D. degree in communication and information systems from Xidian University, Xi'an, Shaanxi, China, in 2020. He was a Visiting Student with the University of Waterloo, Waterloo, ON, Canada, from 2017 to 2018. He is currently an Associate Professor with the School of Information Science and Technology, Dalian Maritime University, Dalian, China. His research interests include resource management and interference coordination for heterogeneous wireless networks and maritime communication systems.

Dewen Yan received the B.Eng. degree from Henan Agricultural University, Zhengzhou, Henan, China, in 2022, and the M.Eng. degree from Dalian Maritime University, Dalian, Liaoning, China, in 2025. He is currently with Beijing Xiaomi Mobile Software Company Ltd., Beijing, China. His research interests include wireless network optimization and resource management.

Ling Lyu (Member, IEEE) received the B.S. degree in telecommunication engineering from Jilin University, Changchun, Jilin, China, in 2013, and the Ph.D. degree in control theory and control engineering from Shanghai Jiao Tong University, Shanghai, China, in 2019. She joined Dalian Maritime University, Dalian, Liaoning, China, in 2019, where she is currently an Associate Professor with the School of Information Science and Technology. She was a Visiting Student with the University of Waterloo, Waterloo, ON, Canada, from 2017 to 2018. Her current research interests include wireless sensor and actuator networks and applications in industrial automation, the joint design of communication and control in industrial cyber-physical systems, estimation and control over lossy wireless networks, machine type communication enabled reliable transmission in the fifth generation network, resource allocation, and energy efficiency.

Yunpeng Ge received the bachelor's degree in electronic information engineering from Shandong University of Technology, Zibo, Shandong, China, in 2024. He is currently pursuing the master's degree with the School of Information Science and Technology, Dalian Maritime University, Dalian, Liaoning, China. His research interests include the coverage optimization of wireless networks.

Nan Cheng (Senior Member, IEEE) received the B.E. and M.S. degrees in information and telecommunications engineering from Tongji University, Shanghai, China, in 2009 and 2012, respectively, and the Ph.D. degree in electrical and computer engineering from the University of Waterloo, Waterloo, ON, Canada, in 2016. He was a Post-Doctoral Fellow with the Department of Electrical and Computer Engineering, University of Toronto, Toronto, ON, Canada, from 2017 to 2019. He is currently a Professor with the State Key Laboratory of Integrated Service Networks and the School of Telecommunications Engineering, Xidian University, Xi'an, Shaanxi, China. He has published over 90 journal articles in IEEE TRANSACTIONS and other top journals. His current research interests include B5G/6G, AI-driven future networks, and space-air-ground integrated networks. He serves as an Associate Editor for IEEE INTERNET OF THINGS JOURNAL, IEEE TRANSACTIONS ON VEHICULAR TECHNOLOGY, IEEE OPEN JOURNAL OF THE COMMUNICATIONS SOCIETY, and *Peer-to-Peer Networking and Applications*, and serves/served as a guest editor for several journals.

Min Sheng (Fellow, IEEE) received the M.S. and Ph.D. degrees in communication and information systems from Xidian University, Xi'an, Shaanxi, China, in 2000 and 2004, respectively. She is currently a Full Professor and the Director of the State Key Laboratory of Integrated Service Networks, Xidian University. Her research interests include mobile ad hoc networks, 5G mobile communication systems, and satellite communications networks. She is a fellow of China Institute of Electronics (CIE) and China Institute of Communications (CIC).

Junyu Liu (Member, IEEE) received the B.Eng. and Ph.D. degrees in communication and information systems from Xidian University, Xi'an, Shaanxi, China, in 2007 and 2016, respectively. He is currently a Full Professor with the State Key Laboratory of Integrated Service Networks, Xidian University. His research interests include wireless coverage and networking technology in heterogeneous networks.

Xuemin (Sherman) Shen (Fellow, IEEE) received the Ph.D. degree in electrical engineering from Rutgers University, New Brunswick, NJ, USA, in 1990.

He is currently a University Professor with the Department of Electrical and Computer Engineering, University of Waterloo, Canada. His research interests include network resource management, wireless network security, the Internet of Things, 5G and beyond, and vehicular networks. He is a registered Professional Engineer of Ontario, Canada, an Engineering Institute of Canada Fellow, a Canadian Academy of Engineering Fellow, a Royal Society of Canada Fellow, a Chinese Academy of Engineering Foreign Member, and an International Fellow of the Engineering Academy of Japan. He received the "West Lake Friendship Award" from Zhejiang Province in 2023, the President's Excellence in Research from the University of Waterloo in 2022, Canadian Award for Telecommunications Research from Canadian Society of Information Theory (CSIT) in 2021, the R.A. Fessenden Award in 2019 from IEEE, Canada, the Award of Merit from the Federation of Chinese Canadian Professionals (Ontario) in 2019, the James Evans Avant Garde Award in 2018 from the IEEE Vehicular Technology Society, the Joseph LoCicero Award in 2015 and Education Award in 2017 from the IEEE Communications Society (ComSoc), the Technical Recognition Award from Wireless Communications Technical Committee in 2019, and the AHSN Technical Committee in 2013. He also received the Excellent Graduate Supervision Award in 2006 from the University of Waterloo and the Premier's Research Excellence Award (PREA) in 2003 from the Province of Ontario, Canada. He served as the General Chair for the 6G Global Conference'2023 and ACM Mobihoc'2015, the Technical Program Committee Chair/Co-Chair for IEEE Globecom'2024, 2016, and 2007, IEEE Infocom'2014, and IEEE VTC'2010 Fall, and the Chair for the IEEE ComSoc Technical Committee on Wireless Communications. He is the Past President of the IEEE ComSoc, the Vice President for Technical and Educational Activities, the Vice President for Publications, a Member-at-Large on the Board of Governors, the Chair of the Distinguished Lecturer Selection Committee, and a member of the IEEE Fellow Selection Committee of the IEEE ComSoc. He served as the Editor-in-Chief for the IEEE INTERNET OF THINGS JOURNAL, IEEE NETWORK, and *IET Communications*.